materials

MDPI

Article

Use of Carbonated Water as Kneading in Mortars Made with Recycled Aggregates

David Suescum-Morales [1], José Ramón Jiménez [1,*] and José María Fernández-Rodríguez [2,*]

[1] Departamento de Ingeniería Rural, Escuela Politécnica Superior de Belmez, Universidad de Córdoba, 14240 Córdoba, Spain; p02sumod@uco.es
[2] Departamento de Química Inorgánica e Ingeniería Química, Escuela Politécnica Superior de Belmez, Universidad de Córdoba, 14240 Córdoba, Spain
* Correspondence: jrjimenez@uco.es (J.R.J.); um1feroj@uco.es (J.M.F.-R.)

Abstract: The increased concern about climate change is revolutionising the building materials sector, making sustainability and environmental friendliness increasingly important. This study evaluates the feasibility of incorporating recycled masonry aggregate (construction and demolition waste) in porous cement-based materials using carbonated water in mixing followed (or not) by curing in a CO_2 atmosphere. The use of carbonated water can be very revolutionary in cement-based materials, as it allows hydration and carbonation to occur simultaneously. Calcite and portlandite in the recycled masonry aggregate and act as a buffer for the low-pH carbonated water. Carbonated water produced better mechanical properties and increased accessible water porosity and dry bulk density. The same behaviour was observed with natural aggregates. Carbonated water results in an interlaced shape of carbonate ettringite (needles) and fills the microcracks in the recycled masonry aggregate. Curing in CO_2 together with the use of carbonated water (concomitantly) is not beneficial. This study provides innovative solutions for a circular economy in the construction sector using carbonated water in mixing (adsorbing CO_2), which is very revolutionary as it allows carbonation to be applied to in-situ products.

Keywords: carbonated water; CO_2 sequestration; accelerated carbonation; circular economy; construction demolition waste

Citation: Suescum-Morales, D.; Jiménez, J.R.; Fernández-Rodríguez, J.M. Use of Carbonated Water as Kneading in Mortars Made with Recycled Aggregates. *Materials* **2022**, *15*, 4876. https://doi.org/10.3390/ma15144876

Academic Editors: Carlos Morón Fernández and Daniel Ferrández Vega

Received: 23 May 2022
Accepted: 8 July 2022
Published: 13 July 2022

1. Introduction

Cement and concrete are used in building and construction work worldwide. The construction industry producing cement and concrete can be regarded as the world's largest industry [1–3]. Construction is responsible for a great amount of CO_2 release [4,5]. One tonne of cement emits approximately 0.6 to 0.8 tonnes of CO_2 [1,6–8]. The CO2 concentration in the atmosphere has increased from 280 to 420 ppm in 2020 [9]. The incorporation of waste and the proper use of resources are leading global challenges to control the negative environmental impact of cement and concrete and preserve the planet.

High-emission countries are actively exploring carbon capture and utilisation (CCU) or storage technologies. CCU is a novel method to reduce CO_2 and turn CO_2 into a commercially interest product [10–12]. The carbonation and chemical reactions in cement-based materials (CBMs) (Equations (1) to (5)) [13–18] occurs with CO_2, affects cement hydration products, and increases $CaCO_3$ production [5,19,20]. As early as 1970, the idea of CO_2 capture through carbonation with CBM appeared [21]. Carbonation of CBM, as an alternate to CCU, reduces water absorption and curing time (useful in the precast industry), increases density, and improves fragmentation resistance and mechanical properties [22–24].

$$Ca(OH)_2 + CO_2 \rightarrow CaCO_3 + H_2O \quad (1)$$

$$C - S - H + CO_2 \rightarrow CaCO_3 + SiO_2 \cdot nH_2O \quad (2)$$

$$4Cao{\cdot}Al_2O_3{\cdot}13H_2O + 4CO_2 \rightarrow 4CaCO_3 + 2Al(OH)_3 + 10H_2O \quad (3)$$

$$3CaO{\cdot}SiO_2 + 3CO_2 + nH_2O \rightarrow SiO_2{\cdot}nH_2O + 3CaCO_3 \quad (4)$$

$$2CaO{\cdot}SiO_2 + 2CO_2 + nH_2O \rightarrow SiO_2{\cdot}nH_2O + 2CaCO_3 \quad (5)$$

The concentration of CO_2 in the environment must be increased for accelerated carbonation in different ways [14,15,18,23–30]. To increase this level of CO_2, a carbonation chamber is usually necessary [13] with or without pressure [31,32], with different levels of CO_2 or even submerging the samples in mixtures of different gases [33–35]. A review on the effect of CO_2 in cement-based materials on the physico-mechanical properties was previously described in another study by Suescum-Morales et al. [36]. The carbonation rate is determined by the diffusion of CO_2 gas in the samples [35]. Carbonation products make samples more dense, preventing the easy entry of CO_2. The need for a high amount of CO_2 in the curing environment implies the need for an accelerated carbonation chamber. An attractive alternative is to apply carbonation technology during cement kneading. To avoid the difficulty of CO_2 diffusion and make CBM carbonation apply to in-situ products, the kneading water is replaced by carbonated water (water with high CO_2 content). Thus, it is possible to start the carbonation simultaneously with the hydration process of the cement and increase carbonation [20,37]. Furthermore, the hydration reaction of the cement occurs much faster than that under normal curing conditions [5].

Construction and demolition waste (CDW) is produced during the demolition phases of several types of construction building or infrastructures (over 30 billion tonnes per year worldwide) [13,38,39]. CDW is composed of several types of waste, in addition to concrete and ceramics, such as glass, stone, bituminous material, and others. Recycled aggregates (RAs) are obtained from CDW with appropriate treatment (recycling plant treatment). A possible simple classification of RA may be made, in a simple way [25]: (i) if the waste is ceramic, the aggregate might be called recycled ceramic aggregates; (ii) if is concrete waste, may be called recycled concrete aggregates (RCA); and (iii) if it is a mixture of the two above, mixed recycled aggregates (MRA) [36,40].

Mixed recycled aggregate (MRA) is the most widely produced RA in the world. The non-existence of regulations and different sources is still limited the use of MRA [41]. Recycled masonry aggregate (RMA) differs from natural aggregates (NAs) mainly in terms water absorption, higher porosity, and lower density [42,43]. MRA has had different uses: as aggregates for masonry mortar, and as an aggregate for alkaline activated material or CBM [41–48]. RMA is a type of MRA obtained from screening and crushing walls waste [36,49–52].

There are two ways to produce accelerated carbonation in RCA [14]: in the aggregate itself [7,42,53–55] or in the mixture of RCA with Portland cement [24,27,28,56]. However, these studies do not investigate the effect of CO_2 on CBMs made with RMA or RCA using carbonated water as kneading water. This research would fill this information gap. Nor has any literature been found that studies the simultaneous use of carbonated water and CO_2 curing.

This study mainly investigates the physico-mechanical properties of a porous CBM with RMA, and carbonated water as kneading water and for subsequent curing in CO_2. To observe the effect of carbonated water on the microstructure of the hardened samples, with NA and RMA, and cured under both regimes, scanning electron microscopy (SEM), energy dispersive X-ray spectroscopy (EDS), and backscattered electron (BSE) were performed. Thermogravimetric analysis and differential thermal analysis (TGA/DTA) was also performed to determine the amount of $CaCO_3$ in all cases. No studies have been found that simultaneously use carbonated water as kneading water, under accelerated curing, and using RMA as aggregate. The production of precast or in-situ non-reinforced CBM products could be possible with the following approach: incorporation of waste (RMA), with the added value to CO_2, and inclusion of carbonated water as kneading water, which can be very revolutionary.

2. Materials and Methods

2.1. Materials

NA was used as a reference. NA and RMA were used in previous research [25,36,49,50]. The components of RMA according to UNE EN 933-11:2009 were: red ceramic bricks (53.9%), masonry mortar (39.8%), unbound aggregates (5.7%), concrete (0.4%), and gypsum particles (0.2%). Water absorption and dry bulk density (DBD) were measured according to UNE-EN 1097-6:2013 [57]. DBD for NA and RMA was 2.63 g·cm^{-3} and 2.14 g·cm^{-3}, respectively. The amount of $CaCO_3$ for NA and RMA (197 and 239 kg/m^3 respectively) was calculated using TGA/DTA. Water absorption was 0.79% for NA and 9% for RMA. CEM II/A-V 42.5 R was used as cement [58] with a DBD of 2.89 g·cm^{-3} according to the characteristics provided by the manufacturer.

As kneading water, two types of commercial water were used: normal water (H_2O) and carbonated water ($CO_2 \cdot H_2O$), both from the manufacturer Fuente Primavera, Spain. For H_2O, the pH value was 7.7 and the initial concentration of CO_2 was between 0.2–0.5 mg·L^{-1}. For $CO_2 \cdot H_2O$, these values were 4.8 (for pH) and 14.1–14.4 mg CO_2·L^{-1}.

2.2. Experimental Design and Curing Conditions

NA and RMA were sieved: 2/4, 1/2, 0.5 /1, 0.25/0.5, 0.125/0.25, and 0/0.125 fractions to reconstitute the lower limit indicated by ASTM C 144-04 [59]. Two gaps were achieved by deleting the following fractions: 0.25/0.5 and <0.125 mm. Its mineral skeleton (with two gaps) can facilitate the input of CO_2 and total carbonation of the mix (more porous). Table 1 shows the reconstituted particle size distribution of NA.

Table 1. Spindle-shaped particle size limits.

Size (mm)	ASTM C 144-04 (Limit)	Fraction Size	Original Percentage Retained	Application of 2 Gaps	Particle Size Distribution Obtained (Passing)
4	100	>4	0	0	100
2	88	2/4	12	16	84
1	62	1/2	26	35	49
0.5	32	0.5/1	30	40	9
0.25	8	**0.25/0.5**	24	0	9
0.125	1	0.125/0.25	7	9	0
0.075	0	**<0.125**	1	0	0
0.063		**TOTAL**	100	100	-

Equations (6) and (7) calculate the dry mass of each component:

$$Dry\ mass\ of\ cement = \frac{V \cdot 1 \cdot \rho_{rd\ cement}}{6} \quad (6)$$

$$Dry\ mass\ of\ NA = \frac{V \cdot 5 \cdot \rho_{rd\ natural\ aggregate}}{6} \quad (7)$$

where $\rho_{rd\ cement}$ = 2.89 g/cm^3 and $\rho_{rd\ natural\ aggregate}$= 2.63 g/cm^3, which are the DBD of cement and NA, respectively. A volume (V) of 1600 cm^3 was manufactured in each mix. According to Equation (7), the mass of NA was 3507 g. The mass of each fraction for NA (Table 2) were obtained according to the 2 gap realized in Table 1. A total substitution of NA by RMA in volume fraction by fraction was realized. To replace NA by RMA, the bulk density was used [60].

Table 2. Aggregate weights used by different fractions.

Mixes	NA			RMA 100%	
Fraction Size (mm)	**Weight Used (g)**	**BD * (g/cm^3)**	**Volume (cm^3)**	**BD * (g/cm^3)**	**Weight Used (g)**
>4	**0**	-	-	-	**-**
2/4	**561**	1.44	388.38	0.99	**386**
1/2	**1216**	1.49	813.53	1.05	**855**
0.5/1	**1403**	1.55	900.01	1.17	**1053**
0.25/0.5	**0**	-	-	-	**-**
0.125/0.25	**327**	1.38	235.80	1.19	**279**
<0.125	**0**	-	-	-	**-**
TOTAL	**3507 (Equation (7))**				**2574**

*** BD = Bulk density**.

The samples were subjected to two curing environments (both with 21 ± 2 °C and 65 ± 10% of relative humidity): (i) normal climatic chamber (CC) and (ii) accelerated carbonation chamber (CO_2·C). For the CC, the CO_2 concentration was 0.04%, and for the CO_2·C it was 5%. The CO_2 used for this condition was provided by Linde (99.99995% purity). Figure 1 shows the experimental design carried out.

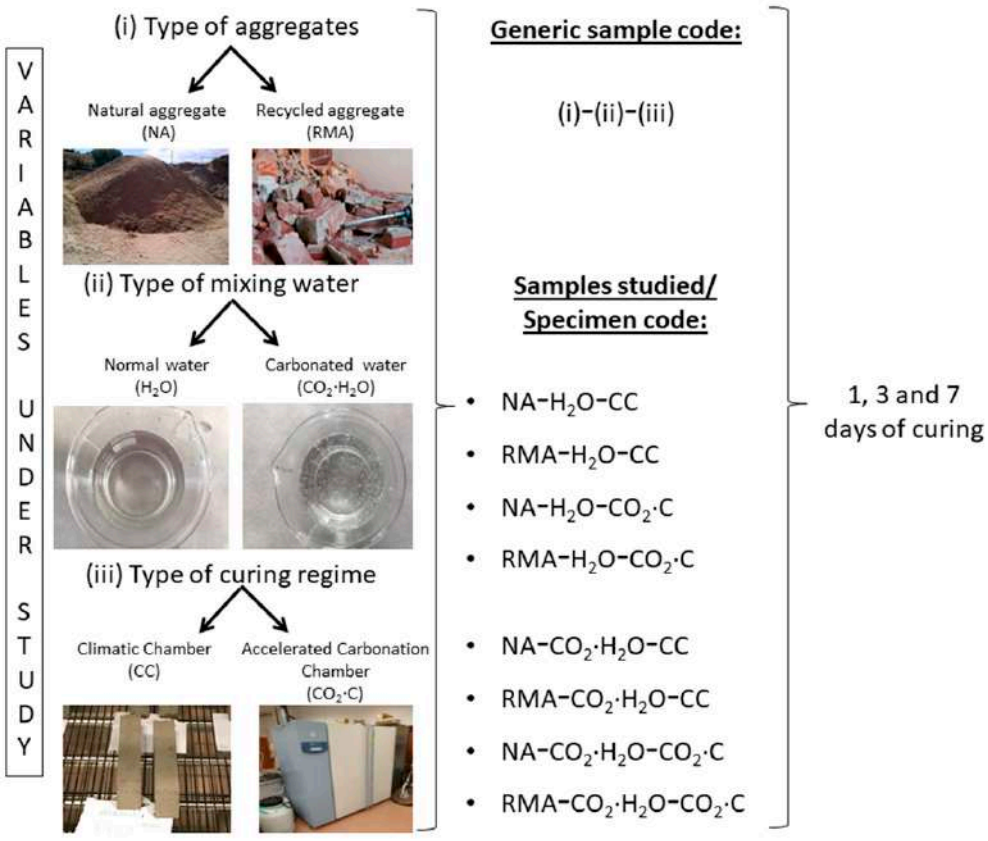

Figure 1. Experimental design carried out.

2.3. Kneading Process

Table 3 shows the composition of the mixes studied. The aggregates were pre-saturated, according to the water absorption of each one of them (NA or RMA). Therefore the w/c ratio used can be considered as effective. The kneading process was in accordance with previous research [25,36].

Table 3. Weights used for the different mixes (g).

Mortar Type	NA	RMA	Cement	Saturation Water		Effective Water		Total Water	w/c	Consistency Index (mm)
				H_2O	$CO_2 \cdot H_2O$	H_2O	$CO_2 \cdot H_2O$			
NA-H_2O-(*)	3507	-	771	28	-	308	-	336	0.4	80 ±10
RMA-H_2O-(*)	-	2574	771	232	-	308	-	540	0.4	80 ±10
NA-$CO_2 \cdot H_2O$-(*)	3507	-	771	-	28	-	308	336	0.4	80 ±10
RMA-$CO_2 \cdot H_2O$-(*)	-	2574	771	-	232	-	308	540	0.4	80 ±10

(*) CC or CO_2-C.

Prismatic 40 × 40 × 160 mm casts were used [61]. The samples were keep in the mould for 3 h. The samples were covered to prevent CO_2 input/output during this time. After this time (3 h), the samples were demoulded because the aim was to demould the samples very quickly, similar to what happens in a precast plant. According to Pan et al. [35], this pre-curing time is crucial to avoid water-saturated capillary pores resulting in a low penetration rate of CO_2 for the samples cured in $CO_2 \cdot C$. The samples were then cured in two chambers: CC and $CO_2 \cdot C$ for 1, 3, and 7 days of curing.

2.4. Test Methods

X-ray fluorescence spectrometry analysis (XRF) was realized with ZSX PRIMUS IV, Rigaku equipment. A Bruker D8 Discover A 25 diffractometer were used for to obtain X-ray diffraction (XRD) patterns. A CuKα radiation (λ = 1.54050 Å; 40 Kv; 30 mA) was used and scan angles between 10° to 70° (2θ) were programmed. The speed used was of 0.02 2θ min^{-1}. For identifying the diffractograms, the International Database ICDD 2003 was used [62].

TGA/DTA were performed using a Setaram Setys Evolution 16/18 instrument with a resolution of 0.002–0.02 µg. The heating increase was 5° min^{-1}.

The flexural (FS) and compressive strength (CS) were obtained according to the European Standard EN 1015-11 [61] for 1, 3, and 7 d of curing. The dry bulk density (DBD) of hardened samples was determined according to European Standard EN 1015-10 [63]. Accessible porosity for water (APW) were measured according to European Standard UNE 83980 [64].

The morphology and composition of the mixes with NA and RMA under the CC regime were studied using H_2O and $CO_2 \cdot H_2O$. SEM, EDS, and BSE were obtained using JEOL JSM 7800F at the age of 7 d. The objective was to observe the effect of carbonated water on the microstructure of the hardened samples, with NA and RMA cured under CC regime. They were then sputtered with gold to obtain the maximum image quality.

All the above tests were carried out in triplicate.

3. Results and Discussion

3.1. Characterization of Raw Materials

Figure 2 shows the XRD patterns of NA, RMA, and cement. Quartz (SiO_2) (05-0490) [62] was the main phase for NA and RMA. Other minority phases were also found and were described in greater detail in other research [25,36]. The diffractogram of the cement was in agreement with the finding of other authors [65–69]. Table 4 shows the XRF results found for NA, RMA, and cement, which are in agreement with the phases found in XRD.

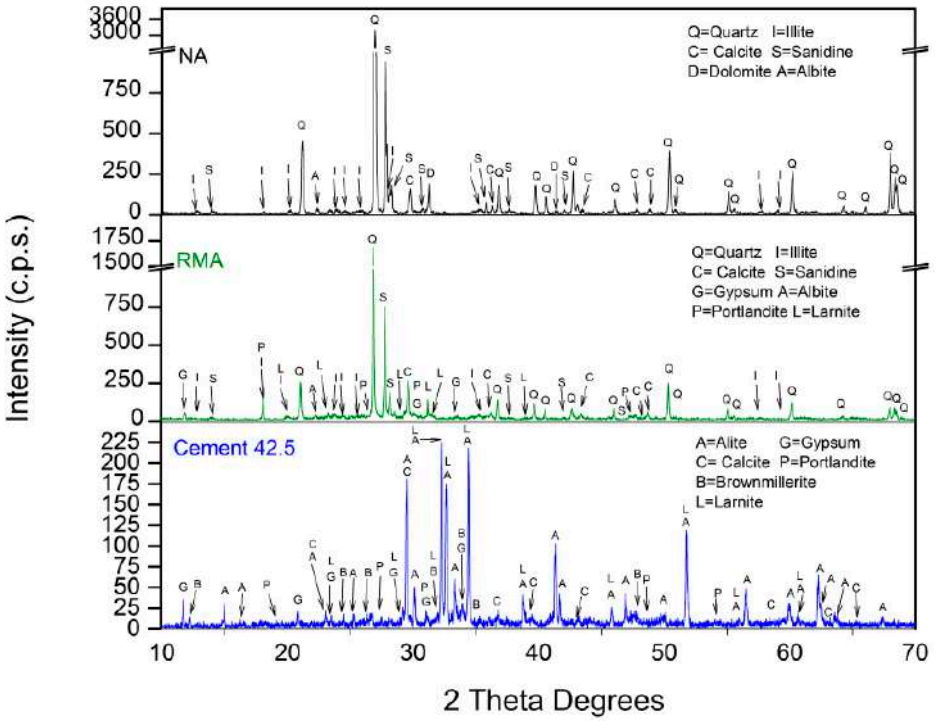

Figure 2. XRD patterns of NA, RMA, and cement.

Table 4. XRF results for NA, RMA, and Cement.

Oxides	NA	RMA	Cement
F_2O	-	0.74	-
Na_2O	0.82	0.71	0.29
MgO	1.06	1.65	1.00
Al_2O_3	5.82	10.79	6.59
SiO_2	49.63	34.44	18.29
P_2O_5	0.07	0.12	0.13
SO_3	0.03	2.52	4.02
Cl_2O_3	-	0.05	0.07
K_2O	1.52	2.18	1.09
CaO	5.60	12.18	45.61
TiO_2	0.27	0.54	0.41
Cr_2O_3	0.04	0.02	-
MnO_2	0.04	0.06	0.05
Fe_2O_3	1.74	3.55	2.85
CuO	-	-	0.04
ZnO	-	0.02	0.02
SrO	-	0.03	0.05
Rb_2O	-	-	0.01
BaO	0.03	0.03	0.06
BALANCE CO_2	32.32	30.61	19.43
TOTAL	67.68	69.39	80.57

3.2. Compressive and Flexural Strength

Figure 3 shows the CS results for the four mixes and two curing regimes at ages of 1, 3, and 7 days of curing. When comparing NA-H_2O-CC with NA-CO_2·H_2O-CC at 1 day of age, CS decreased by 8.6%. According to Valdemir dos Santos et al. [20], this result is related to the reduced AFm formation in the microstructure during the early hydration period [20]. Similar results were reported by Lippiatt et al. [5] in a cement paste aged 1 d using carbonated water. In addition, the low pH value of carbonated water (4.8) can negatively affect the strength [70], delay the setting [71], and produce changes

in the cement paste structure [72]. It is possible that a low pH leads to the reduction of hydrated calcium silicate and hydrated calcium aluminate because the reactions of equations 8–10 occur. Additionally, the amount of Portlandite present decreases. Therefore, the structure of the cement paste will be weaker. Nevertheless, at 3 and 7 d, an increment of 18% and 12.5% was obtained, respectively, when using carbonated water for the NA mixture and CC regime. When kneading cement and water, the pH increases rapidly, and this solution becomes saturated with $Ca(OH)_2$ after 24 h [73,74]. Furthermore, the calcite phase found in NA (Figure 2) can act as a buffer when added to carbonated water, as observed by Lippiatt et al. [5] to achieve simultaneous hydration and carbonation in cement. This saturated solution of $Ca(OH)_2$, together with CO_2 in the carbonated water, favoured the carbonation reaction and increased CS at 3 and 7 d [22–24]. Equations (8)–(10) show the chemical reaction with carbonated water [20].

$$CO_{2(gaseous)} + 2OH^-{}_{(gaseous)} \leftrightarrow CO_3{}^{2-}{}_{(aqueous)} + H_2O_{(liquid)} \quad (8)$$

$$Ca(OH)_{2(aqueous)} \leftrightarrow Ca^{2+}{}_{(aqueous)} + 2OH^-{}_{(aqueous)} \quad (9)$$

$$Ca^{2+}{}_{(aqueous)} + CO_3{}^{2-}{}_{(aqueous)} + H_2O_{(liquid)} \leftrightarrow CaCO_{3(solid)} + H_2O_{(liquid)} \quad (10)$$

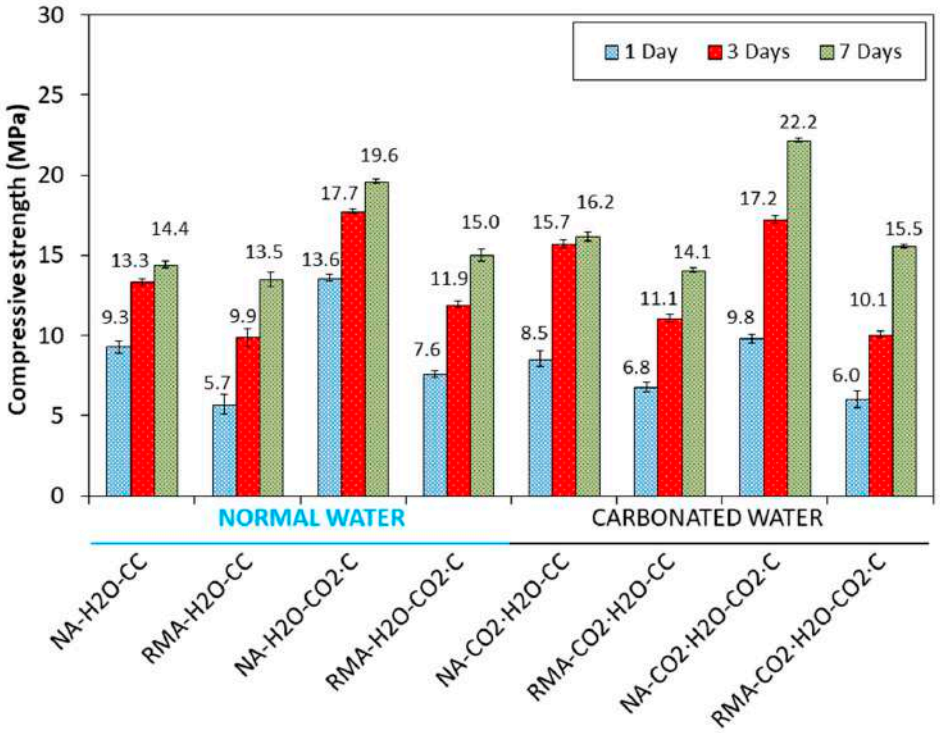

Figure 3. Compressive strength at different curing ages and hardening environments.

Compared to NA, RMA mixture under CC regime, using carbonated and normal water (RMA-H_2O-CC and RMA-CO_2·H_2O-CC), had slightly lower CS. This loss of mechanical properties agreed with other studies when the percentage of substitution of NA for RA was 100% [14,75–79]. However, compared to normal water, the carbonated water was beneficial in this case for all ages of curing (19.3%, 12.1%, and 4.4% for 1, 3, and 7 d, respectively) due to the presence of $CaCO_3$ and $Ca(OH)_2$ in RMA (Figure 2). These phases act as a buffer of carbonated water [5], increase pH, avoid the loss of mechanical resistance, and delay hydration [70,71] that occur in the mixture with NA with 1 d of curing. Thus, carbonated water with RMA can improve the mechanical strength under the CC regime.

For NA and RMA mixtures, the increase in CS in samples cured with CO_2·C (NA-H_2O-CC vs. NA-H_2O-CO_2·C and RMA-H_2O-CC vs. RMA-H_2O-CO_2·C) agree with the

results in [13,14,18,24,27,28,56,80–82]. For NA mixtures, with 1 d and under CO_2·C, when using carbonated water in the kneading, compared with normal water, decreased the CS by 38.77% (NA-H_2O-CO_2·C vs. NA-CO_2·H_2O-CO_2·C). The low pH value of carbonated water along with accelerated carbonation (CO_2·C) results in a negative effect on strength [70] and delayed setting [71], which lowers the pH values of the mix [83–85]. For 3 d of curing, the effect of carbonated water on CS was still negative. For 7 d of curing, an increment of 13.3% was observed. This could indicate the regulation of pH [22–24] and the carbonation of the sample.

The same behaviour was observed in the samples with RMA (RMA-H_2O-CO_2·C vs. RMA-CO_2·H_2O-CO_2·C), although with minor decreases for 1 and 3 d. This is again due to $CaCO_3$ and $Ca(OH)_2$ in RMA (Figure 2) acting as a buffer of carbonated water [5], maintaining a pH higher than that with NA. Thus, carbonated water under accelerated carbonation (with NA and RMA) is beneficial only after 7 d of curing.

The FS results for all the mixes under CC and CO_2-C at the ages of 1, 3, and 7 d, in Figure 4, reveal the same trend as CS.

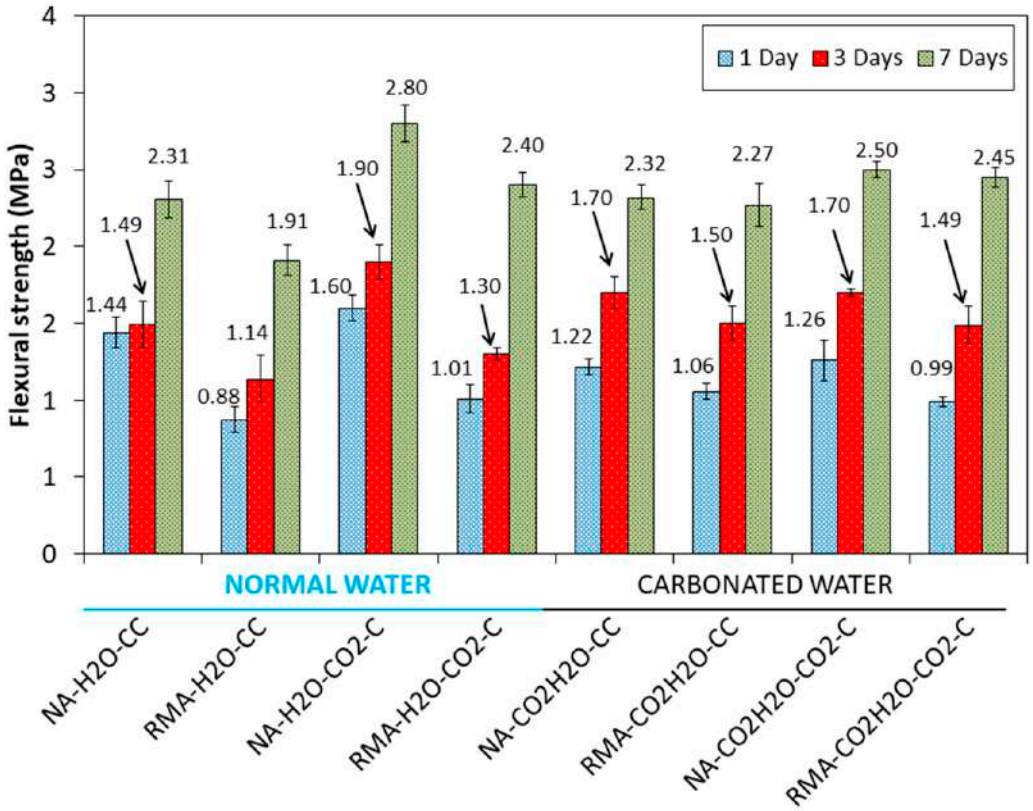

Figure 4. Flexural strength at different curing ages and hardening environments.

3.3. DBD and APW

DBD and APW are shown in Figure 5 for 7 d of curing under CC and CO_2·C. On the NA mixture, under the CC regime, the use of carbonated water as kneading water, compared with normal water, incremented the DBD by 3.3%. This result agrees with the increase in the mechanical properties in Figures 3 and 4. Carbonated water favours the carbonation reaction at 7 d of curing, increasing the DBD [22–24]. The APW also increased by 5.28% when using carbonated water during kneading. This result is in accordance with Valdemir et al. [20], who found that CO_2 released by the carbonated water could generate additional porosity. The same behaviour was observed with RMA (RMA-H_2O-CC and RMA-CO_2·H_2O-CC), in which DBD increased by 0.8% and APW by 19.06%.

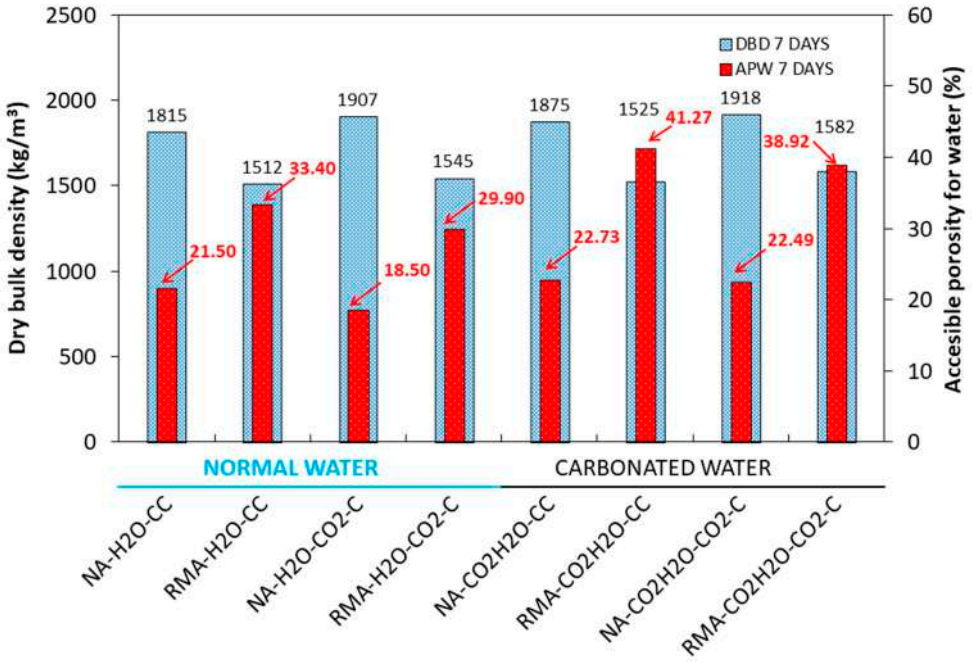

Figure 5. DBD and APW for 7 d under CC and CO_2·C.

For the RMA mixture under the CC regime, when using carbonated and normal water (RMA-H_2O-CC and RMA-CO_2·H_2O-CC), DBD and APW were higher than those in the same mixtures with NA. This agrees with the lower particle dry density, and higher water absorption of RMA reported in [51,79,86].

For the NA and RMA mixtures, using normal water, an increase in DBD and a decrease in APW were observed for samples cured in CO_2·C (NA-H_2O-CC vs. NA-H_2O-CO_2·C and RMA-H_2O-CC vs. RMA-H_2O-CO_2·C). These mechanical properties could be due to sample carbonation, as observed in [13,14,18,24,27,28,56,80]. Carbonated water for kneading water under accelerated carbonation, compared to normal water, increased the DBD and APW (NA-H_2O-CO_2·C vs. NA-CO_2·H_2O-CO_2·C and RMA-H_2O-CO_2·C vs. RMA-CO_2·H_2O-CO_2·C). These results agree with the mechanical properties observed in Figures 3 and 4.

3.4. XRD

XRD obtained for NA using normal and carbonated water as kneading water under CC are shown in Figure 6. For normal water at 1 d, the main phases found were quartz (05-0490) [62], calcite (05-0586) [62], dolomite (11-0078), albite (10-0393) [85], and microline (19-0926) [84], which agrees with the fundamental composition of NA in Figure 2. Hatrurite (86-0402) [62], larnite (33-0302) [62] from the cement used (Figure 2), portlandite (44-1481) [62], and ettringite (37-1479) [62] from the reaction products of Ordinary Portland cement (OPC) [87,88] were also observed. Comparing the phases found using normal or carbonated water as kneading water, a sharp decrease of the phases hatrurite and larnite were observed (Inset Figure 6 labelled "C_3S and C_2S", red colour "1 day normal water", purple colour "1 day carbonated water"). Furthermore, the formation of portlandite $Ca(OH)_2$ was affected by the carbonated water as kneading water (Inset Figure 7 labelled "Portlandite", red colour "1 day normal water", purple colour "1 day carbonated water") and is in accordance with Equation (7). The loss of intensity of hatrurite and larnite peaks and delay in the formation of portlandite were also reported by Hou et al. [71] with acid water. The observed results can be because of the pH of the carbonated water (4.8) and decreased mechanical strength at 1 d of curing, as shown in Figures 4 and 5.

Comparing the diffractogram of 1 d with those obtained at the ages of 3 and 7 d for carbonated water, the same phases were identified but an increase in the intensity was observed in the calcite phase (Inset Figure 6 labelled "$CaCO_3$ (3 days)" and "$CaCO_3$ (7 days)"),

suggesting that carbonated water as kneading water produced carbonation [22–24]. This also explains the increased mechanical strength in Figures 3 and 4 and DBD in Figure 5.

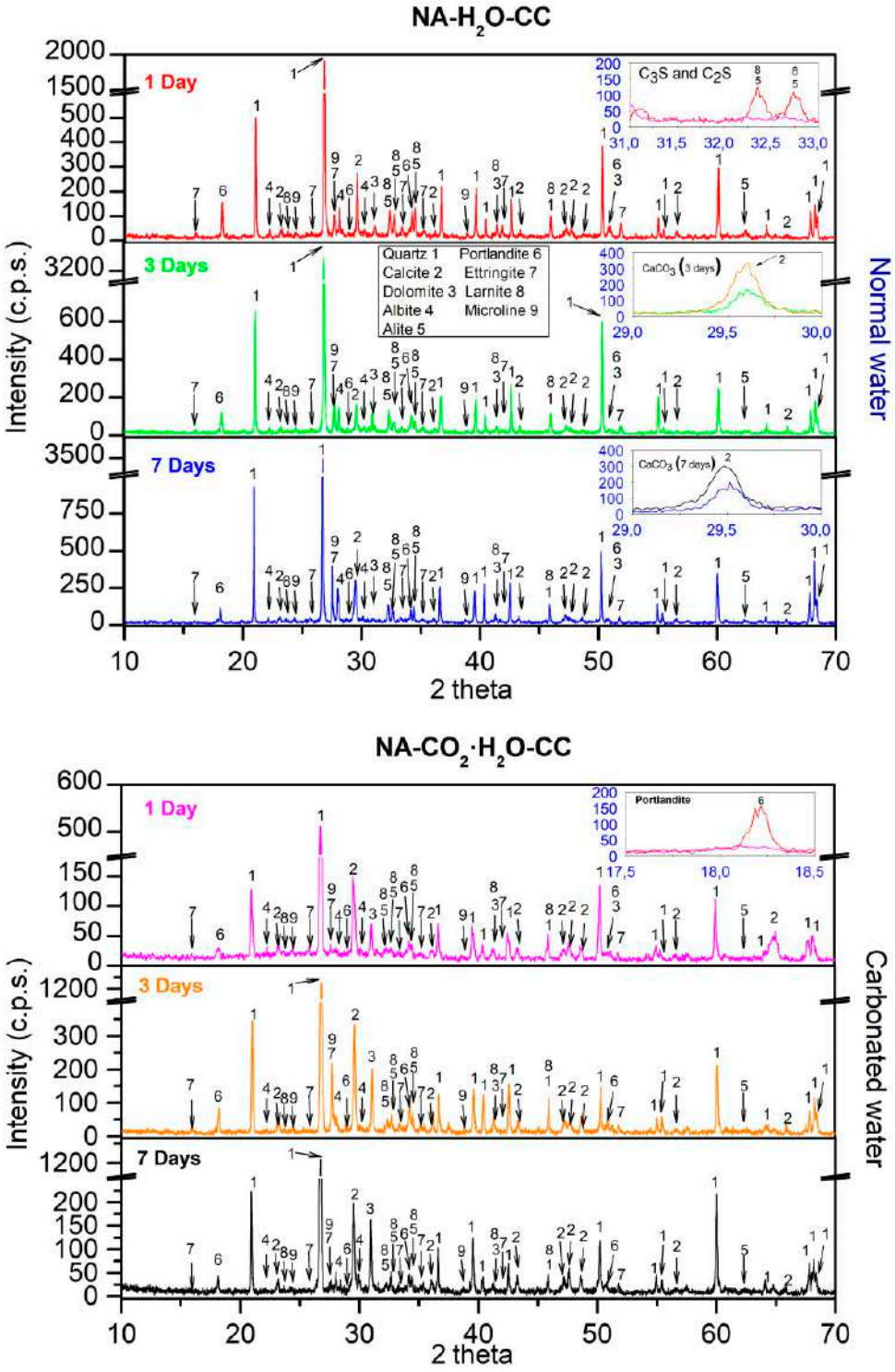

Figure 6. XRD for NA with normal and carbonated water under CC.

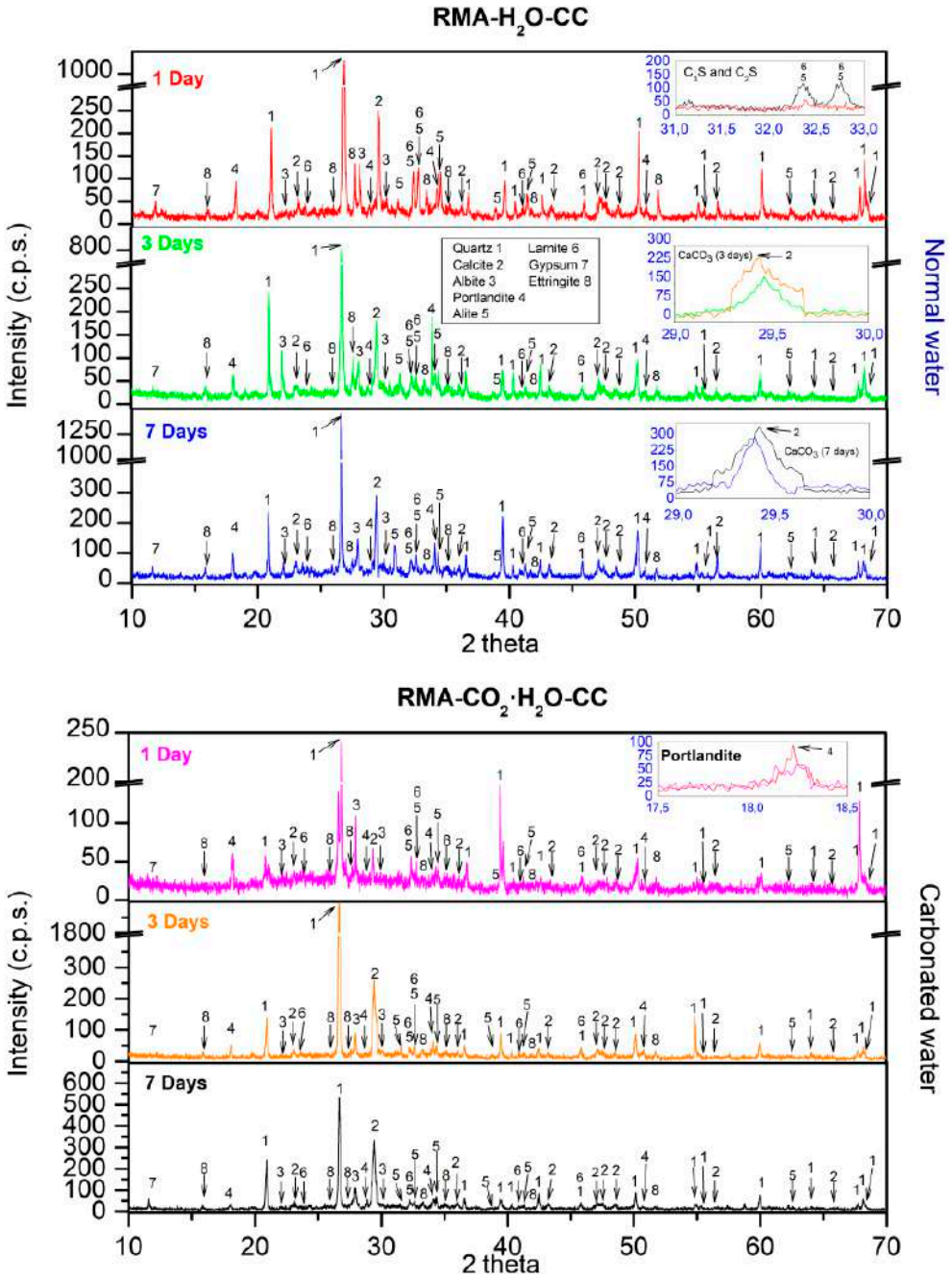

Figure 7. XRD for RMA with normal and carbonated water under CC.

XRD obtained for NA using normal and carbonated water as kneading water under CC are shown in Figure 7. With carbonated water (Figure 7 inset labelled "C_3S and C_2S"), we observed a decrease in the peaks of the phases hatrurite and larnite. In addition, the formation of portlandite $Ca(OH)_2$ was not significantly delayed when using carbonated water (Figure 8 inset labelled "Portlandite"). Both processes were due to the presence of $CaCO_3$ and $Ca(OH)_2$ in RMA (Figure 2). These phases acted as a buffer [5]. Hence, carbonated water can increase the mechanical properties at 1 d of age with RMA than with NA (Figures 3 and 4). These results highlight that RMA, acting as a buffer for carbonated water during kneading, avoids a decrease in pH without adding $CaCO_3$ or $Ca(OH)_2$, as previously proposed in [5,89]. Owing to its mineralogical composition, RMA has a similar effect as $CaCO_3$ and $Ca(OH)_2$.

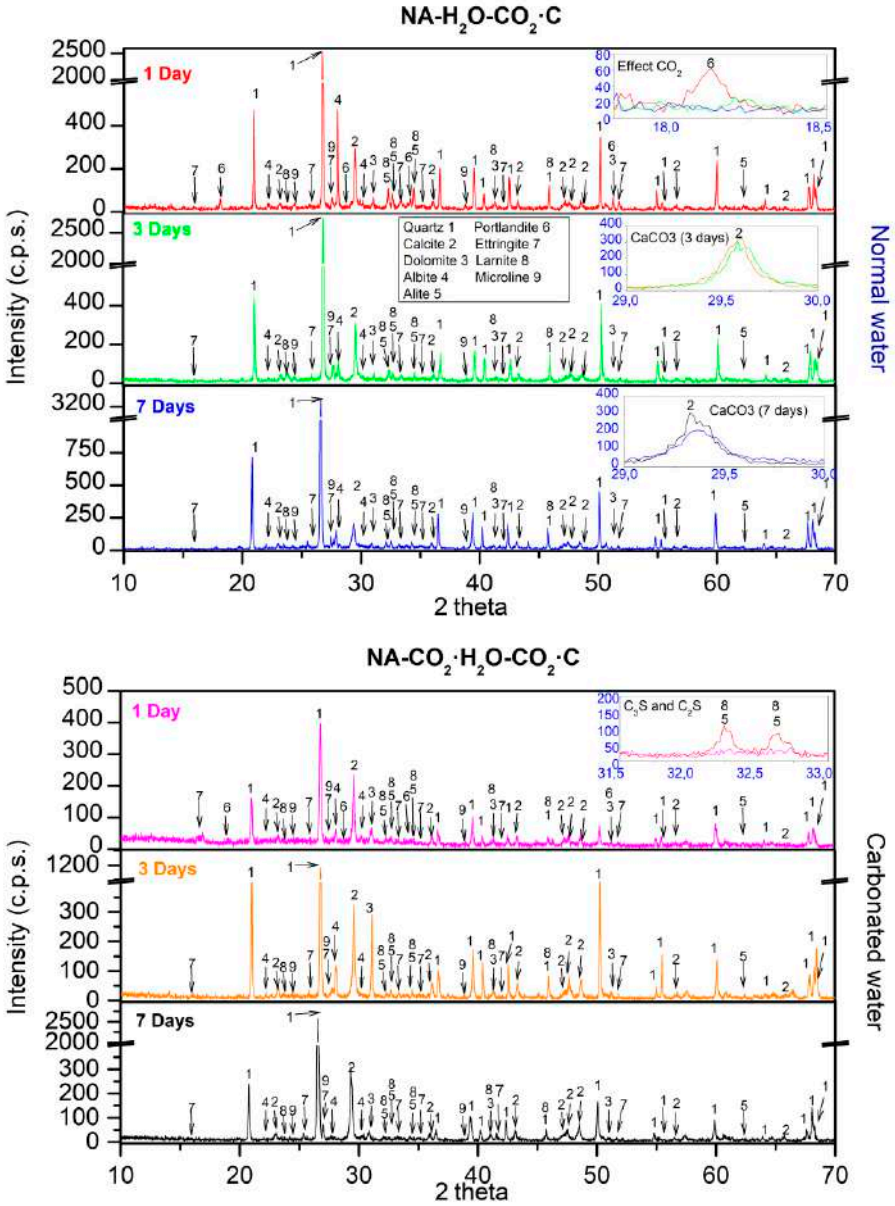

Figure 8. XRD for NA with normal and carbonated water under CO_2·C.

At 3 and 7 d with normal water, the same phases were identified as that of 1 d. Comparing these diffractograms with that obtained for 3 and 7 d using carbonated water, a higher intensity was observed in the calcite peaks (Figure 7 inset labelled "$CaCO_3$ (3 days)" and "$CaCO_3$ (7 days)"). This behaviour was already observed in the samples with NA (Figure 7) and indicates that the carbonated water produced carbonation [22–24]. This supports the increase in mechanical strength with carbonated water (in Figures 3 and 4) and DBD (in Figure 5).

XRD obtained for NA using normal and carbonated water as kneading water under CO_2·C are shown in Figure 8. For 1 d, with normal water, the same phases as in CC were found. For 3 and 7 d, the disappearance of the portlandite phase was observed (Figure 8 inset labelled "Effect CO_2"), which shows the consumption portlandite when it comes into contact with CO_2 (Equation (1)). This concurs with an increase in the mechanical strength in samples cured in CO_2·C (Figures 3 and 4). This was due to samples carbonation, as reported in [13,14,18,24,27,28,56,80]. The same phases were found for 1, 3, and 7 d with carbonated water. The portlandite also disappeared at the age of 3 and 7 d.

The effect of carbonated water at 1 d, under the CO_2·C regime, is almost the same as that under CC (Figure 6). However, a decrease in the peaks of the hatrurite and larnite phases were observed (Figure 8 inset labelled "C_3S and C_2S"). For 3 d, the effect of carbonated water (Figure 6) is negligible on the calcite formed with respect to the effect produced by the carbonation chamber (Figure 8), because the amount of CO_2 contributed by the CO_2·C regime is greater than that of the carbonated water (Figure 8 inset labelled "$CaCO_3$ (3 days)", similar intensity found for $CaCO_3$ peaks). These results agree with the delay in setting [71] and strength development [70] due to the initial decrease in pH produced by combining carbonated water and CO_2-C regimes. At 7 d, a greater intensity was observed in the calcite phase, more with carbonated water than with normal water (Figure 8 inset labelled "$CaCO_3$ (7 days)"). This indicates that pH had been regulated [22–24] and that carbonation of the sample is better than in with normal water and agrees with the results of the mechanical properties in Figures 4 and 5 and DBD in Figure 6.

XRD obtained for RMA using normal and carbonated water as kneading water under CO_2·C are shown in Figure 9. At 1 d, with normal water, the phases found were the same as those found in the CC regime (Figure 7). For 3 and 7 d, the disappearance of the portlandite phase was observed (Figure 9 inset labelled "Effect CO_2"), indicating carbonation (Equation (1)) [13–17].

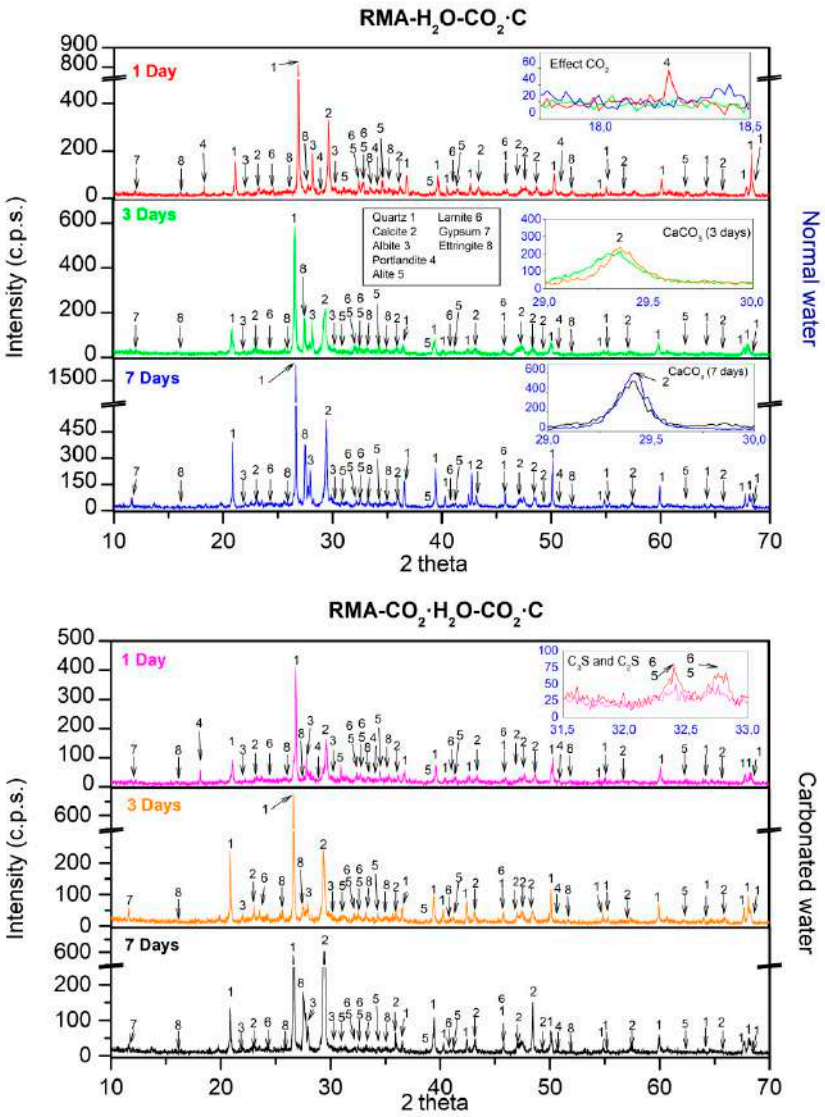

Figure 9. XRD for RMA with normal and carbonated water under CO_2·C.

With carbonated water, the same phases were observed as that with normal water. For 1 d, a light decrease of hatrurite and larnite were observed (Figure 9 inset labelled "C_3S and C_2S", red colour "1 day normal water", purple colour "1 day carbonated water"), indicating that carbonated water has a retarding effect on the development of mechanical properties at a young age. As with NA (Figure 8), the same behaviour, including calcite peak intensities, was observed at the age of 3 d (Figure 9 inset labelled "$CaCO_3$ (3)"). The low pH value of carbonated water along with accelerated carbonation (CO_2·C) which also lowers the pH, negatively affects the strength, although less in the case of NA (Figures 3 and 4). At 7 d of curing, the calcite peaks were similar with carbonated and normal water (Figure 9 inset labelled "$CaCO_3$ (7)") and agree with the mechanical properties in Figures 3 and 4 and DBD in Figure 5.

3.5. SEM

Figure 10 shows a general SEM and elemental composition mapping of the NA mixture with normal and carbonated water as kneading water under CC at low magnification (NA-H_2O-CC vs. NA-CO_2·H_2O-CC). Two main zones were detected: siliceous aggregate and cement paste. The main element in the aggregates is Si and agrees with the chemical composition (Table 4), XRD (Figure 2) results. The main elements contained in the cement paste were Ca, Al, K, and Mg. At low magnification, no differences were observed using carbonated water.

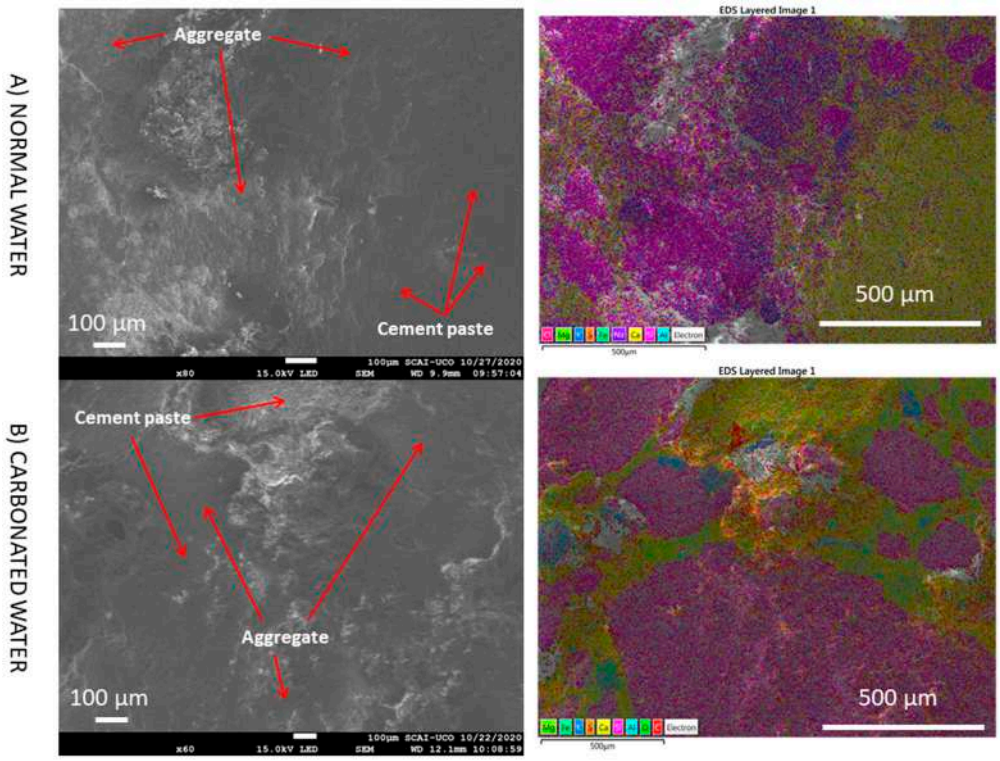

Figure 10. SEM images and elemental composition mapping of NA with normal and carbonated water under normal curing regime CC (NA-H_2O-CC vs. NA-CO_2·H_2O-CC) at low magnification.

However, by increasing the magnification over the cement paste zone, significant differences were found when using carbonated water (Figure 11). First, it seems that the structure of the cement paste with carbonated water was more porous than that obtained with normal water. The qualitative analysis by SEM agrees with the highest APW found with carbonated water (Figure 5). With normal water, it can be seen that the grains with rounded faces and edges were formed around the cement particles. Nevertheless, with carbonated water, large amounts of well-developed and intertwined needles particles, with very high surface areas are observed. Considering the morphological similarities with

ettringite $Ca_6[Al(OH)_6]_2$ $(SO_4)_3 \cdot 26H_2O$, it can be speculated that the needle-like structure is a carbonated ettringite with the chemical formula $Ca_6[Al(OH)_6]_2$ $(CO)_3 \cdot 26H_2O$ [37]. Because of the high CO_2 content of carbonated water, ion exchange occurs; that is, SO_4^{2-} is fully or partially replaced by CO_3^{2-}. A similar result was found by Pingping et al. [27] with water curing with CO_2.

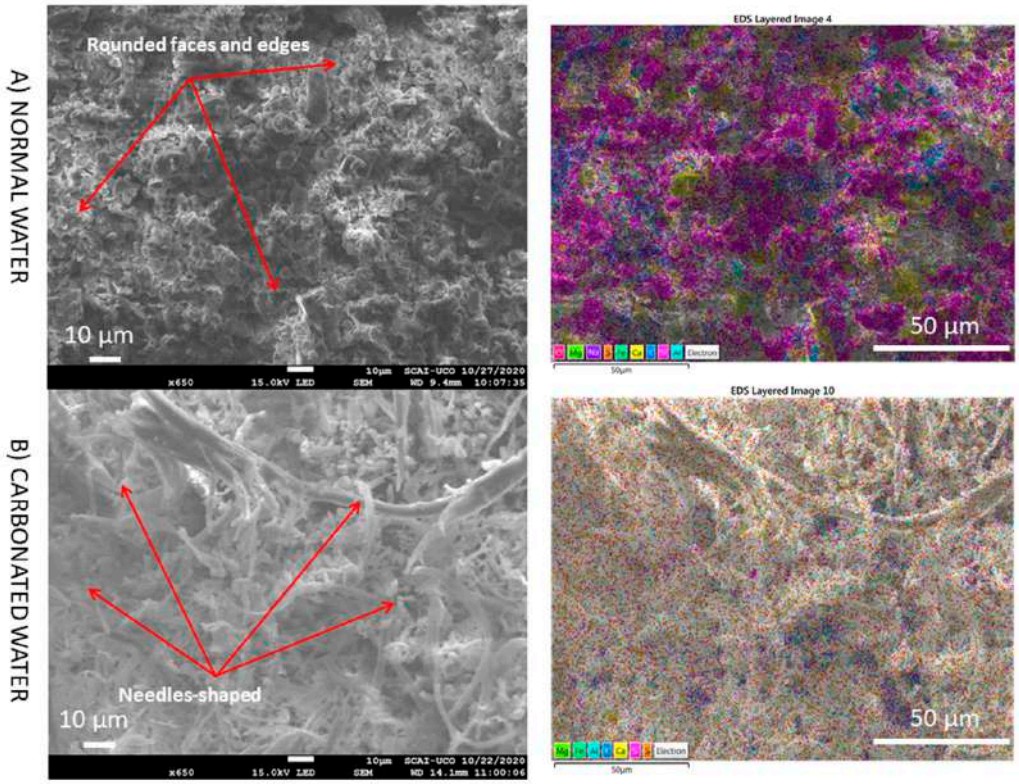

Figure 11. SEM images and elemental composition mapping of NA (zone cement paste) with normal and carbonated water under normal curing regime CC (NA-H_2O-CC vs. NA-$CO_2 \cdot H_2O$-CC) at medium magnification.

SEM images with higher magnification were taken to confirm the above results (Figure 12). With normal water, grains with rounded faces and edges were observed. However, with carbonated water, hexagonal- or orthorhombic-shaped (1) and needle-shaped particles (2) were observed. EDS analysis of the hexagonal particle revealed the presence of Ca, C, and O, indicating the possibility of $CaCO_3$ [2,27]. This agrees with the greater intensity of calcite observed in XRD with carbonated water for NA (Figure 6 vs. Figure 7). For needle-shaped particles, EDS revealed a high concentration of C and O, indicating that SO_4^{2-} was fully or partially replaced by CO_3^{2-} to form carbonate ettringite [37]. Boumaza et al. [19] formed carbonated crystals having hexagonal or orthorhombic shapes between the needles of ettringite under a CO_2 environment. The interlaced shape of the carbonate ettringite and greater presence of calcite (due to the carbonation produced by CO_2 in the carbonated water) improved the mechanical properties (Figures 3 and 4) compared to normal water.

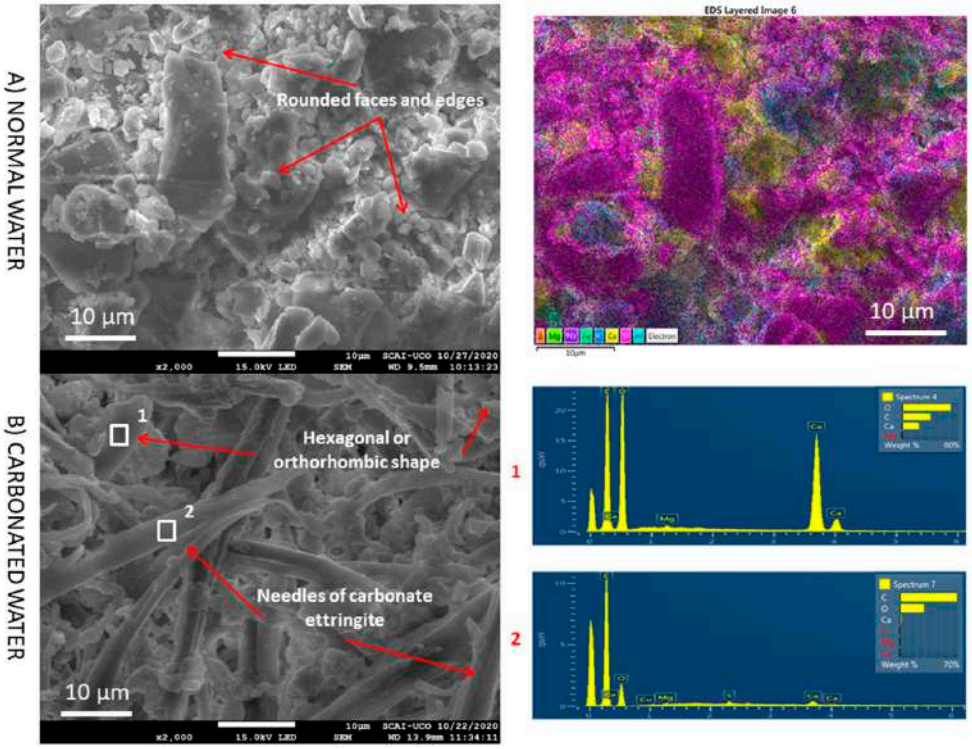

Figure 12. SEM images and EDS of NA (zone cement paste) with normal and carbonated water under normal curing regime CC (NA-H_2O-CC vs. NA-CO_2·H_2O-CC) at high magnification. Elemental composition mapping.

Figure 13 shows a general SEM and elemental composition mapping of the RMA mixture with normal and carbonated water under CC at low magnification (RMA-H_2O-CC vs. RMA-CO_2·H_2O-CC). In this case, two zones were observed: a siliceous aggregate or piece of brick, which is in accordance with the nature of the RMA (Figure 2), and cement paste containing Ca, Al, K, and Mg as the main elements. Furthermore, microcracks and a possible interfacial transition zone (ITZ), which is the area between the old and the new cement paste and is the weakest region in MRA mortar [3,90,91], were observed. These could explain the decrease in mechanical properties (Figures 3 and 4) with the replacement of NA by RMA (with normal and carbonated water under CC) and the higher porosity found with RMA (Figure 5). At this magnification, no differences were found between carbonated and normal water with RMA. The same areas as with normal water are also found. This is contrary to what is observed with NA (Figure 10).

With slightly higher magnification, microcracks were more visible (Figure 14). There were fewer microcracks when using carbonated water as the carbonatation products ($CaCO_3$ particles) can gradually fill pores and micropores [22–24,35]. This agrees with the improvement in the mechanical properties observed with carbonated water in RMA under the CC regime (RMA-H_2O-CC vs. RMA-CO_2·H_2O-CC). Furthermore, this increase in carbonation products was also observed in the XRD analysis (Figure 7). Notably, when using RMA and carbonated water, the presence of carbonated ettringite was not observed, unlike when using NA (Figures 11 and 12) due to the existence of calcite and portlandite in RMA (Figure 2). Calcite and portlandite act as buffers for carbonated water [5], consuming CO_2 from carbonated water, especially portlandite (Equation (1)), thereby avoiding the full or partial replacement of SO_4^{2-} by CO_3^{2-}.

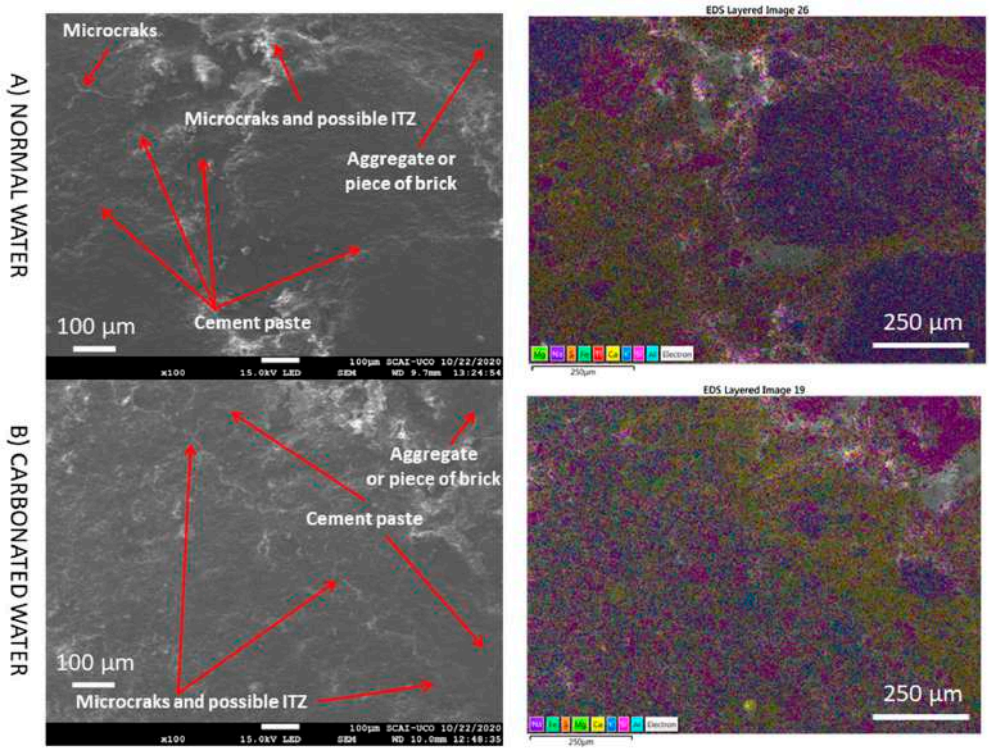

Figure 13. SEM images and elemental composition mapping of RMA with normal and carbonated water under normal curing regime CC (RMA-H_2O-CC vs. RMA-$CO_2 \cdot H_2O$-CC) at low magnification.

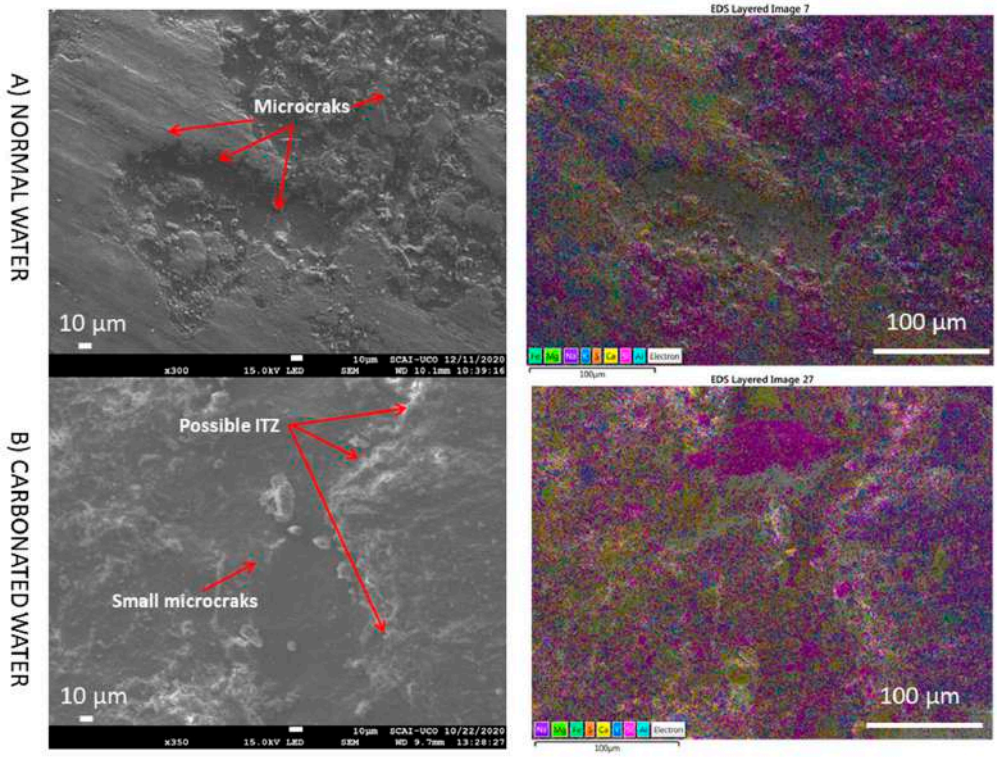

Figure 14. SEM images and elemental composition mapping of RMA with normal and carbonated water under normal curing regime CC (RMA-H_2O-CC vs. RMA-$CO_2 \cdot H_2O$-CC) at medium magnification.

At higher magnification (Figure 15), no microcracks were observed due to the filling of microcracks by the effect of carbonated water in the RMA. In addition, carbonate ettringite

(needle-shaped particles) is not observed. The same behaviour was observed at very high magnification (Figure 16). Therefore, carbonated water on the microstructure of RMA serves the purpose of filling the microcracks. Studies on the influence of carbonated water with RMA have not been found in the literature.

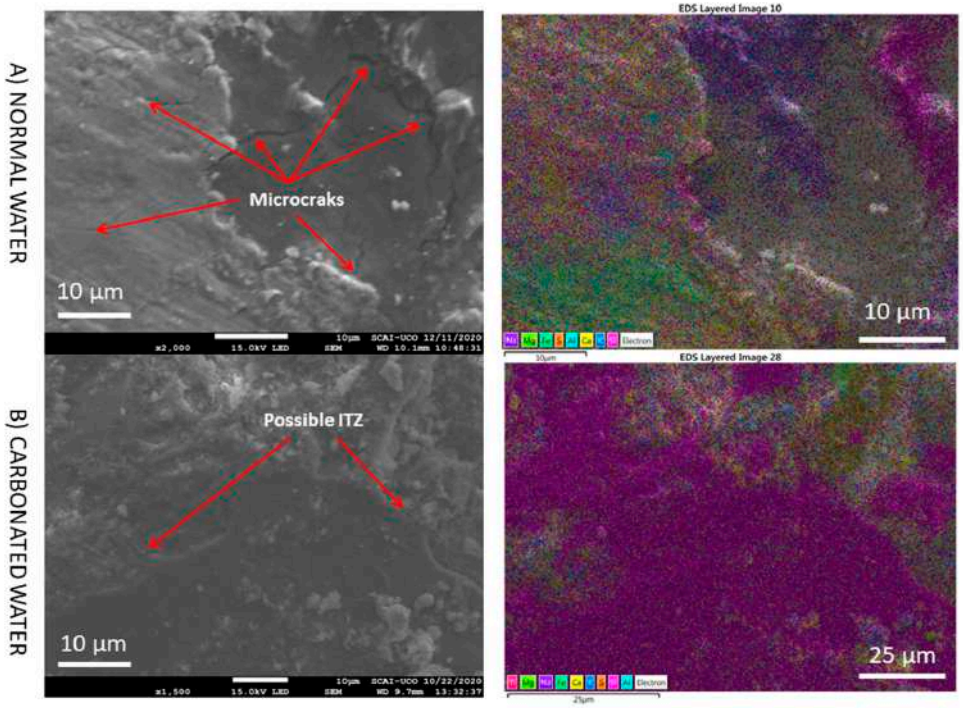

Figure 15. SEM images and elemental composition mapping of RMA with normal and carbonated water under normal curing regime CC (RMA-H_2O-CC vs. RMA-$CO_2 \cdot H_2O$-CC) at high magnification.

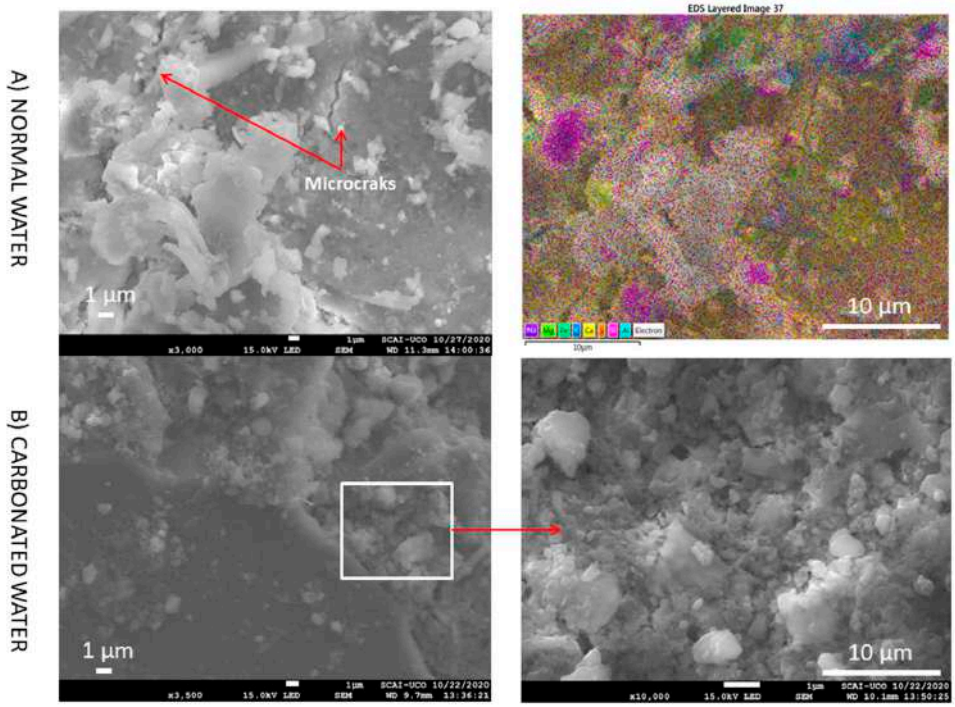

Figure 16. SEM images and elemental composition mapping of RMA with normal and carbonated water under normal curing regime CC (RMA-H_2O-CC vs. RMA-$CO_2 \cdot H_2O$-CC) at very high magnification.

3.6. TGA-DTA

To determine whether carbonated water produces a greater amount of $CaCO_3$ in the mixes with NA and RMA in CC regime, TGA/DTA was performed (Figure 17). Five stages were observed for all the mixes with normal and carbonated water. In the stage from 480 to 1000 °C, $CaCO_3$ decomposition occurred [2,56], attributed to the loss of mass resulting from calcium carbonate decomposition. A high loss of mass in this range indicates high calcium carbonate in the mix.

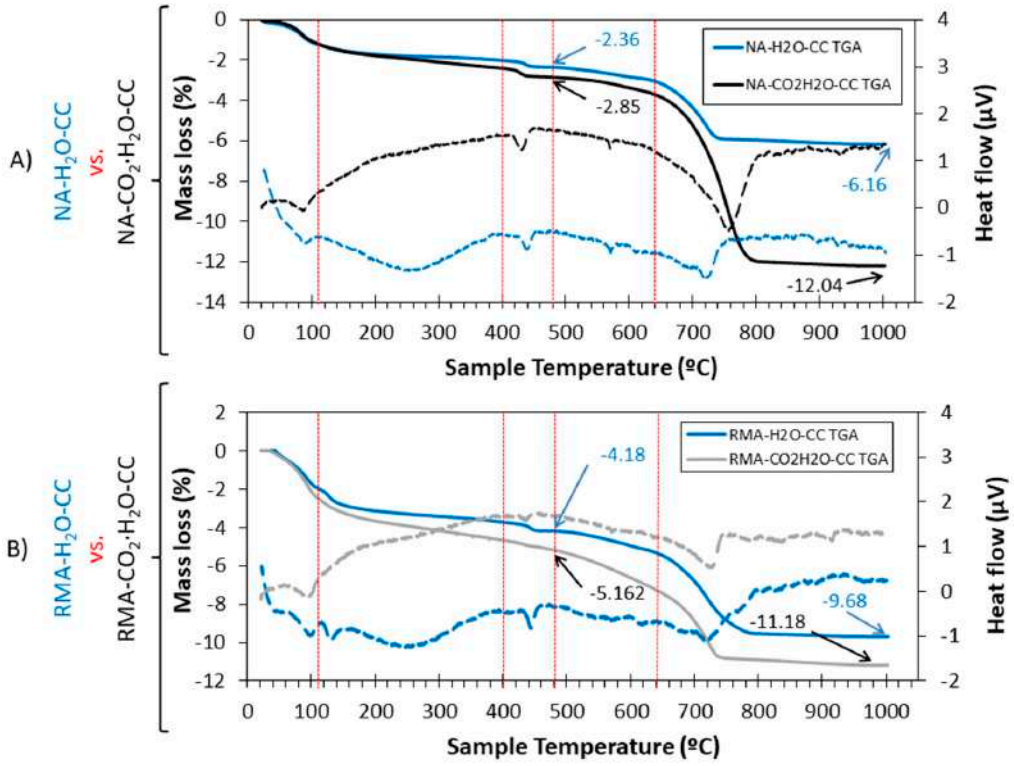

Figure 17. TGA (solid lines) and DTA (dotted lines) curves for (**A**) mix with NA and (**B**) mix with RMA. Use of normal and carbonated water.

For the mix with NA (Figure 17A), a mass loss of 3.8% and 9.19% were observed for normal and carbonated water, respectively, (NA-H_2O-CC vs. NA-CO_2·H_2O-CC) in the range of 480–1000 °C, indicating a greater amount of $CaCO_3$ (product of carbonation) formation with carbonated water. This is in agreement with the mechanical properties (Figures 3 and 4), DBD (Figure 6), XRD results (Figure 6), and SEM (Figures 10–12). The temperature of the decomposition peak of $CaCO_3$ is different between NA-H_2O-CC and NA-CO_2·H_2O-CC. This was due to the different "nature" of $CaCO_3$. In the case of NA-H_2O-CC, this $CaCO_3$ is the result of the hardening process of the cement [36,92]. In the case of NA-CO_2·H_2O-CC, the calcium carbonate is the result of the carbonation produced in the sample and by them exist a delayed in the decomposition temperature. In contrast, for the mix with RMA (Figure 17B), the mass loss is 5.5 and 6.01 for normal and carbonated water, respectively (RMA-H_2O-CC vs. RMA-CO_2·H_2O-CC), between 480 and 1000 °C. In this case, the difference in calcium carbonate formation was not as important as in NA (although it is still greater with carbonated water than with normal water). This was already described in the analysis of the intensity for calcite peaks in XRD. The difference between the intensity of the peaks was greater in the NA mixture than in the RMA mixture, at the age of 7 d (see Figure 6 inset labelled "$CaCO_3$ (7 days)" vs. Figure 7 inset labelled "$CaCO_3$ (7 days)").

4. Conclusions

This study presents an experimental study using carbonated water as kneading water and its impact on the physical-mechanical properties of a porous CBM made with NA and RMA. The main objective was to evaluate the influence of carbonated water together with whether or not subsequent curing in carbonation chamber on the mechanical properties and explain this behaviour using XRD, SEM, and TGA/DTA. The characterisation of the mix composition with different aggregates (NA or RMA), normal water or carbonated water as kneading water, and different hardening environments (different level of CO_2) were performed at 1, 3, and 7 d. The following conclusions were obtained:

- Carbonated water worsened mechanical properties at 1 d of curing with NA under the CC regime, compared to normal water. The phases of $CaCO_3$ and $Ca(OH)_2$ in the RMA, acted as a buffer for carbonated water.
- The low pH value of carbonated water and accelerated carbonation (CO_2·C) further lowers the pH, and negatively affects the strength at 1 d of normal curing for all the mixes. The simultaneous utilization of carbonated water as kneading water and subsequent curing in CO_2 is not recommended.
- In all the mixtures studied, the effect of carbonated water increased the DBD (due to carbonation) and APW, indicating that carbonated water generated additional porosity. The carbonation reaction that occurs with carbonated water under CC explains the increase in mechanical strength at 7 d of curing for NA and RMA. A greater intensity in the $CaCO_3$ peaks (XRD) and increased weight loss of calcite decomposition (TGA/DTA) was also observed.
- The presence of interlaced needles of ettringite carbonate observed by SEM and the increased presence of calcite (due to the carbonation produced by CO_2 in the carbonated water) resulted in better mechanical properties than normal water. Carbonated water on the microstructure of the RMA results in the filling of microcracks (shown in the SEM images). Ettringite carbonate was not observed in this case because of portlandite in RMA, which consumed CO_2 from carbonated water. Carbonated water as kneading water using RMA could allow for the production of precast CBM products with good mechanical properties without the need for CO_2 curing chamber.

The utilization of carbonated water as kneading water in CBM with recycled aggregates (circular economy) can be a novel and interesting procedure to obtain a more environmentally friendly building material without the use of a carbonation chamber. At the same time, it improves mechanical properties and contributes to climate change mitigation.

Author Contributions: Conceptualization, D.S.-M. and J.M.F.-R.; Methodology, J.R.J.; writing—original draft preparation, D.S.-M.; writing—review and editing, J.M.F.-R. and J.R.J.; supervision, J.M.F.-R.; project administration, J.M.F.-R. and J.R.J. All authors have read and agreed to the published version of the manuscript.

Funding: This research was funded by Andalusian regional government UCO-FEDER 20 research project (Ref. 1381172-R) and the Ministry of Science and Innovation of the Government of Spain through the PRECAST-CO2 research project (Ref. PID2019-111029RB-I00).

Institutional Review Board Statement: Not applicable.

Informed Consent Statement: Not applicable.

Data Availability Statement: Not applicable.

Acknowledgments: D. Suescum-Morales acknowledges funding from MECD-Spain (http://www.mecd.gob.es/educacion-mecd/) FPU 17/04329. D. Suescum-Morales also want to thank Cesar Javier Ramos and Maria Esther Jiménez for their help in measuring the initial CO_2 concentration of normal and carbonated water.

Conflicts of Interest: The authors declare no conflict of interest.

References

1. Lippiatt, N.; Ling, T.-C.; Pan, S.-Y. Towards carbon-neutral construction materials: Carbonation of cement-based materials and the future perspective. *J. Build. Eng.* **2020**, *28*, 101062. [CrossRef]
2. Zhan, B.J.; Xuan, D.; Poon, C.S.; Shi, C.J. Mechanism for rapid hardening of cement pastes under coupled CO_2-water curing regime. *Cem. Concr. Compos.* **2019**, *97*, 78–88. [CrossRef]
3. Wang, R.; Yu, N.; Li, Y. Methods for improving the microstructure of recycled concrete aggregate: A review. *Constr. Build. Mater.* **2020**, *242*, 118164. [CrossRef]
4. Burek, J.; Nutter, D. Life cycle assessment of grocery, perishable, and general merchandise multi-facility distribution center networks. *Energy Build.* **2018**, *174*, 388–401. [CrossRef]
5. Lippiatt, N.; Ling, T.-C.; Eggermont, S. Combining hydration and carbonation of cement using super-saturated aqueous CO_2 solution. *Constr. Build. Mater.* **2019**, *229*, 116825. [CrossRef]
6. Higuchi, T.; Morioka, M.; Yoshioka, I.; Yokozeki, K. Development of a new ecological concrete with CO_2 emissions below zero. *Constr. Build. Mater.* **2014**, *67*, 338–343. [CrossRef]
7. Sanjuán, M.; Andrade, C.; Mora, P.; Zaragoza, A. Carbon Dioxide Uptake by Mortars and Concretes Made with Portuguese Cements. *Appl. Sci.* **2020**, *10*, 646. [CrossRef]
8. Kaliyavaradhan, S.K.; Ling, T.-C.; Mo, K.H. CO_2 sequestration of fresh concrete slurry waste: Optimization of CO_2 uptake and feasible use as a potential cement binder. *J. CO2 Util.* **2020**, *42*, 101330. [CrossRef]
9. Yuan, J. Vertical Profiles of Carbon Dioxide in the Lower Troposphere at Manua Loa Observatory, Hawaii, Determined with a Multi-Copter Drone. In Proceedings of the Ocean Sciences Meeting, San Diego, CA, USA, 16–21 February 2020.
10. Qiu, R.; Zhang, H.; Zhou, X.; Guo, Z.; Wang, G.; Yin, L.; Liang, Y. A multi-objective and multi-scenario optimization model for operation control of CO_2-flooding pipeline network system. *J. Clean. Prod.* **2020**, *247*, 119157. [CrossRef]
11. Yu, S.; Horing, J.; Liu, Q.; Dahowski, R.; Davidson, C.; Edmonds, J.; Liu, B.; McJeon, H.; McLeod, J.; Patel, P.; et al. CCUS in China's mitigation strategy: Insights from integrated assessment modeling. *Int. J. Greenh. Gas Control* **2019**, *84*, 204–218. [CrossRef]
12. Suescum-Morales, D.; Cantador-Fernández, D.; Jiménez, J.; Fernández, J. Mitigation of CO_2 emissions by hydrotalcites of Mg_3Al-CO_3 at 0 °C and high pressure. *Appl. Clay Sci.* **2020**, *202*, 105950. [CrossRef]
13. Liang, C.; Pan, B.; Ma, Z.; He, Z.; Duan, Z. Utilization of CO_2 curing to enhance the properties of recycled aggregate and prepared concrete: A review. *Cem. Concr. Compos.* **2019**, *105*, 103446. [CrossRef]
14. Kaliyavaradhan, S.K.; Ling, T.-C. Potential of CO_2 sequestration through construction and demolition (C&D) waste—An overview. *J. CO2 Util.* **2017**, *20*, 234–242. [CrossRef]
15. Lu, B.; Shi, C.; Zheng, J.; Ling, T.-C. Carbon dioxide sequestration on recycled aggregates. In *Carbon Dioxide Sequestration in Cementitious Construction Materials*; Woodhead Publishing: Sawston, UK, 2018. [CrossRef]
16. Quesada Carballo, L.; del Rosario Perez Perez, M.; Cantador Fernandez, D.; Caballero Amores, A.; Fernandez Rodriguez, J.M. Optimum Particle Size of Treated Calcites for CO_2 Capture in a Power Plant. *Materials* **2019**, *12*, 1284. [CrossRef]
17. Hang, J.; Shi, C.; Li, Y.; Pan, X.; Poon, C.-S.; Xie, Z. Performance Enhancement of Recycled Concrete Aggregates through Carbonation. *J. Mater. Civ. Eng.* **2015**, *27*. [CrossRef]
18. Rostami, V.; Shao, Y.; Boyd, A.J. Carbonation Curing versus Steam Curing for Precast Concrete Production. *J. Mater. Civ. Eng.* **2012**, *24*, 1221–1229. [CrossRef]
19. Boumaaza, M.; Huet, B.; Turcry, P.; Aït-Mokhtar, A. The CO_2-binding capacity of synthetic anhydrous and hydrates: Validation of a test method based on the instantaneous reaction rate. *Cem. Concr. Res.* **2020**, *135*, 106113. [CrossRef]
20. Dos Santos, V.; Tonoli, G.H.D.; Mármol, G.; Savastano, H. Fiber-cement composites hydrated with carbonated water: Effect on physical-mechanical properties. *Cem. Concr. Res.* **2019**, *124*, 105812. [CrossRef]
21. Zhang, D.; Ghouleh, Z.; Shao, Y. Review on carbonation curing of cement-based materials. *J. CO2 Util.* **2017**, *21*, 119–131. [CrossRef]
22. Zhan, B.; Poon, C.S.; Liu, Q.; Kou, S.; Shi, C. Experimental study on CO_2 curing for enhancement of recycled aggregate properties. *Constr. Build. Mater.* **2014**, *67*, 3–7. [CrossRef]
23. Kou, S.-C.; Zhan, B.-J.; Poon, C.-S. Use of a CO_2 curing step to improve the properties of concrete prepared with recycled aggregates. *Cem. Concr. Compos.* **2014**, *45*, 22–28. [CrossRef]
24. Shi, C.; He, F.; Wu, Y. Effect of pre-conditioning on CO_2 curing of lightweight concrete blocks mixtures. *Constr. Build. Mater.* **2012**, *26*, 257–267. [CrossRef]
25. Suescum-Morales, D.; Fernández-Rodríguez, J.M.; Jiménez, J.R. Use of carbonated water to improve the mechanical properties and reduce the carbon footprint of cement-based materials with recycled aggregates. *J. CO2 Util.* **2022**, *57*, 101886. [CrossRef]
26. Kashef-Haghighi, S.; Shao, Y.; Ghoshal, S. Mathematical modeling of CO_2 uptake by concrete during accelerated carbonation curing. *Cem. Concr. Res.* **2015**, *67*, 1–10. [CrossRef]
27. He, P.; Shi, C.; Tu, Z.; Poon, C.S.; Zhang, J. Effect of further water curing on compressive strength and microstructure of CO_2-cured concrete. *Cem. Concr. Compos.* **2016**, *72*, 80–88. [CrossRef]
28. Zhan, B.J.; Poon, C.S.; Shi, C.J. Materials characteristics affecting CO_2 curing of concrete blocks containing recycled aggregates. *Cem. Concr. Compos.* **2016**, *67*, 50–59. [CrossRef]
29. Zhan, B.; Poon, C.; Shi, C. CO_2 curing for improving the properties of concrete blocks containing recycled aggregates. *Cem. Concr. Compos.* **2013**, *42*, 1–8. [CrossRef]

30. Liu, S.; Guan, X.; Zhang, S.; Xu, C.; Li, H.; Zhang, J. Sintering red mud based imitative ceramic bricks with CO_2 emissions below zero. *Mater. Lett.* **2017**, *191*, 222–224. [CrossRef]
31. Monkman, S.; Shao, Y. Carbonation Curing of Slag-Cement Concrete for Binding CO_2 and Improving Performance. *J. Mater. Civ. Eng.* **2010**, *22*, 296–304. [CrossRef]
32. Shi, C.; Wu, Y. Studies on some factors affecting CO_2 curing of lightweight concrete products. *Resour. Conserv. Recycl.* **2008**, *52*, 1087–1092. [CrossRef]
33. Ben Ghacham, A.; Pasquier, L.-C.; Cecchi, E.; Blais, J.-F.; Mercier, G. Valorization of waste concrete through CO_2 mineral carbonation: Optimizing parameters and improving reactivity using concrete separation. *J. Clean. Prod.* **2017**, *166*, 869–878. [CrossRef]
34. Pan, X.; Shi, C.; Farzadnia, N.; Hu, X.; Zheng, J. Properties and microstructure of CO_2 surface treated cement mortars with subsequent lime-saturated water curing. *Cem. Concr. Compos.* **2019**, *99*, 89–99. [CrossRef]
35. Pan, X.; Shi, C.; Hu, X.; Ou, Z. Effects of CO2 surface treatment on strength and permeability of one-day-aged cement mortar. *Constr. Build. Mater.* **2017**, *154*, 1087–1095. [CrossRef]
36. Suescum-Morales, D.; Kalinowska-Wichrowska, K.; Fernández, J.M.; Jiménez, J.R. Accelerated carbonation of fresh cement-based products containing recycled masonry aggregates for CO_2 sequestration. *J. CO2 Util.* **2021**, *46*, 101461. [CrossRef]
37. Kwasny, J.; Basheer, P.A.M.; Russell, M.; Doherty, W.; Owens, K.; Ward, N. CO_2 sequestration in cement-based materials during mixing process using carbonated water and gaseous CO_2. In Proceedings of the 4th International Conference on the Durability of Concrete Structures, West Lafayette, IN, USA, 24–26 July 2014; pp. 72–79. [CrossRef]
38. Li, Y.; Fu, T.; Wang, R. An assessment of microcracks in the interfacial transition zone of recycled concrete aggregates cured by CO_2. *Constr. Build. Mater.* **2020**, *236*, 117543. [CrossRef]
39. Amin, M.; Tayeh, B.A.; Agwa, I.S. Effect of using mineral admixtures and ceramic wastes as coarse aggregates on properties of ultrahigh-performance concrete. *J. Clean. Prod.* **2020**, *273*, 123073. [CrossRef]
40. Tam, V.W.Y.; Soomro, M.; Evangelista, A.C.J. A review of recycled aggregate in concrete applications (2000–2017). *Constr. Build. Mater.* **2018**, *172*, 272–292. [CrossRef]
41. Ferreira, R.L.S.; Anjos, M.A.S.; Maia, C.; Pinto, L.; de Azevedo, A.R.G.; de Brito, J. Long-term analysis of the physical properties of the mixed recycled aggregate and their effect on the properties of mortars. *Constr. Build. Mater.* **2020**, *274*, 121796. [CrossRef]
42. Pavlu, T.; Fortova, K.; Divis, J.; Hajek, P. The Utilization of Recycled Masonry Aggregate and Recycled EPS for Concrete Blocks for Mortarless Masonry. *Materials* **2019**, *12*, 1923. [CrossRef]
43. Mora-Ortiz, R.S.; Munguía-Balvanera, E.; Díaz, S.A.; Magaña-Hernández, F.; Del Angel-Meraz, E.; Bolaina-Juárez, Á. Mechanical Behavior of Masonry Mortars Made with Recycled Mortar Aggregate. *Materials* **2020**, *13*, 2373. [CrossRef]
44. Cuenca-Moyano, G.M.; Martín-Pascual, J.; Martín-Morales, M.; Valverde-Palacios, I.; Zamorano, M. Effects of water to cement ratio, recycled fine aggregate and air entraining/plasticizer admixture on masonry mortar properties. *Constr. Build. Mater.* **2020**, *230*, 116929. [CrossRef]
45. Tan, J.; Cai, J.; Li, X.; Pan, J.; Li, J. Development of eco-friendly geopolymers with ground mixed recycled aggregates and slag. *J. Clean. Prod.* **2020**, *256*, 120369. [CrossRef]
46. Cantero, B.; del Bosque, I.S.; Matías, A.; Medina, C. Statistically significant effects of mixed recycled aggregate on the physical-mechanical properties of structural concretes. *Constr. Build. Mater.* **2018**, *185*, 93–101. [CrossRef]
47. Zhang, L.; Sojobi, A.; Kodur, V.; Liew, K.M. Effective utilization and recycling of mixed recycled aggregates for a greener environment. *J. Clean. Prod.* **2019**, *236*, 117600. [CrossRef]
48. Cantero, B.; Bravo, M.; de Brito, J.; del Bosque, I.S.; Medina, C. Mechanical behaviour of structural concrete with ground recycled concrete cement and mixed recycled aggregate. *J. Clean. Prod.* **2020**, *275*, 122913. [CrossRef]
49. Jiménez, J.R.; Ayuso, J.; López, M.; Fernández, J.M.; De Brito, J.M.C.L. Use of fine recycled aggregates from ceramic waste in masonry mortar manufacturing. *Constr. Build. Mater.* **2013**, *40*, 679–690. [CrossRef]
50. Ledesma, E.F.; Jiménez, J.R.; Ayuso, J.; Fernández, J.M.; de Brito, J. Maximum feasible use of recycled sand from construction and demolition waste for eco-mortar production–Part-I: Ceramic masonry waste. *J. Clean. Prod.* **2015**, *87*, 692–706. [CrossRef]
51. Silva, R.; de Brito, J.; Dhir, R. Performance of cementitious renderings and masonry mortars containing recycled aggregates from construction and demolition wastes. *Constr. Build. Mater.* **2016**, *105*, 400–415. [CrossRef]
52. Silva, Y.F.; Robayo, R.A.; Mattey, P.E.; Delvasto, S. Properties of self-compacting concrete on fresh and hardened with residue of masonry and recycled concrete. *Constr. Build. Mater.* **2016**, *124*, 639–644. [CrossRef]
53. Pacheco, J.; de Brito, J.; Chastre, C.; Evangelista, L. Experimental investigation on the variability of the main mechanical properties of concrete produced with coarse recycled concrete aggregates. *Constr. Build. Mater.* **2019**, *201*, 110–120. [CrossRef]
54. Silva, R.V.; Jiménez, J.; Agrela, F.; de Brito, J. Real-scale applications of recycled aggregate concrete. In *New Trends in Eco-efficient and Recycled Concrete*; Woodhead Publishing: Sawston, UK, 2018; pp. 573–589. [CrossRef]
55. Lopez-Uceda, A.; Ayuso, J.; Jiménez, J.R.; Galvín, A.P.; Del Rey, I. Feasibility study of roller compacted concrete with recycled aggregates as base layer for light-traffic roads. *Road Mater. Pavement Des.* **2018**, *21*, 276–288. [CrossRef]
56. Sáez del Bosque, I.F.; Van den Heede, P.; De Belie, N.; de Rojas, M.S.; Medina, C. Carbonation of concrete with construction and demolition waste based recycled aggregates and cement with recycled content. *Constr. Build. Mater.* **2020**, *234*, 117336. [CrossRef]
57. *UNE-EN-1097-6:2013*; Tests for Mechanical and Physical Properties of Aggregates. Part 6: Determination of Particle Density and Water Absorption. CEN: Brussels, Belgium, 2013.

58. *UNE-EN-197-1:2011*; Part 1: Composition, Specifications and Conformity Criteria for Common Cements. BSI: London, UK, 2011.
59. *ASTM-C-144*; Standard Specification for Aggregate for Masonry Mortar. American Society for Testing and Materials: West Conshohocken, PA, USA, 2004.
60. *EN-1015-6:1999*; Methods of Test Mortar for Mansory. Part 6: Determination of Bulk Density of Fresh Mortar. SIST: Ljubljana, Slovenia, 1999.
61. *EN-1015-11:2000*; Methods of Test for Mortar for Mansory. Part 11: Determination of Flexural and Compressive Strenght of Hardened Mortar. SIS: Stockholm, Sweden, 2000.
62. JCPDS. Joint Committee on Power Diffraction Standard-International Centre for Diffraction. 2003.
63. *EN-1015-10:2000*; Methods of Test Mortar for Mansory. Part 6: Determination of Bulk Density of Hardened Mortar. AENOR: Madrid, Spain, 2000.
64. *UNE-83980:2014*; Concrete Durability. Test Methods. Determination of the Water Absorption, Density and Accesible Porosity for Water in Concrete. Spanish Association for Standardization: Madrid, Spain, 2014.
65. Roncero, J.; Valls, S.; Gettu, R. Study of the influence of superplasticizers on the hydration of cement paste using nuclear magnetic resonance and X-ray diffraction techniques. *Cem. Concr. Res.* **2002**, *32*, 103–108. [CrossRef]
66. Tang, S.; Cai, X.; He, Z.; Shao, H.; Li, Z.; Chen, E. Hydration process of fly ash blended cement pastes by impedance measurement. *Constr. Build. Mater.* **2016**, *113*, 939–950. [CrossRef]
67. Abed, M.; Nemes, R.; Lublóy, E. Performance of Self-Compacting High-Performance Concrete Produced with Waste Materials after Exposure to Elevated Temperature. *J. Mater. Civ. Eng.* **2020**, *32*, 05019004. [CrossRef]
68. Suescum-Morales, D.; Ríos, J.D.; De La Concha, A.M.; Cifuentes, H.; Jiménez, J.R.; Fernández, J.M. Effect of moderate temperatures on compressive strength of ultra-high-performance concrete: A microstructural analysis. *Cem. Concr. Res.* **2021**, *140*, 106303. [CrossRef]
69. Esquinas, R.; Motos-Pérez, D.; Jiménez, M.; Ramos, C.; Jiménez, J.R.; Fernández, J. Mechanical and durability behaviour of self-compacting concretes for application in the manufacture of hazardous waste containers. *Constr. Build. Mater.* **2018**, *168*, 442–458. [CrossRef]
70. Sumra, Y.; Payam, S.; Zainah, I. The pH of Cement-based Materials: A Review. *J. Wuhan Univ. Technol. Sci. Ed.* **2020**, *35*, 908–924. [CrossRef]
71. Hou, W.; Bao, J. Evaluation of cement retarding performance of cellulosic sugar acids. *Constr. Build. Mater.* **2019**, *202*, 522–527. [CrossRef]
72. Bao, H.; Xu, G.; Wang, Q.; Peng, Y.; Liu, J. Study on the deterioration mechanism of cement-based materials in acid water containing aggressive carbon dioxide. *Constr. Build. Mater.* **2020**, *243*, 118233. [CrossRef]
73. Li, X.; Shui, Z.; Sun, T.; Liu, K.; Wang, X. The hydration mechanism of cement-based materials served in marine environment during early-age magnesium precipitation. *Constr. Build. Mater.* **2020**, *230*, 117010. [CrossRef]
74. Lothenbach, B.; Winnefeld, F. Thermodynamic modelling of the hydration of Portland cement. *Cem. Concr. Res.* **2006**, *36*, 209–226. [CrossRef]
75. Jiménez, J.R.; Fernández-Ledesma, E.; Ayuso, J.; Corinaldesi, V.; Iglesias, F.J. A proposal for the maximum use of recycled concrete sand in masonry mortar design. *Mater. Construcción* **2016**, *66*, e075. [CrossRef]
76. Duan, Z.; Hou, S.; Xiao, J.; Li, B. Study on the essential properties of recycled powders from construction and demolition waste. *J. Clean. Prod.* **2020**, *253*, 119865. [CrossRef]
77. Martínez, P.S.; Cortina, M.G.; Martínez, F.F.; Sánchez, A.R. Comparative study of three types of fine recycled aggregates from construction and demolition waste (CDW), and their use in masonry mortar fabrication. *J. Clean. Prod.* **2016**, *118*, 162–169. [CrossRef]
78. Gonzalez-Corominas, A.; Etxeberria, M. Properties of high performance concrete made with recycled fine ceramic and coarse mixed aggregates. *Constr. Build. Mater.* **2014**, *68*, 618–626. [CrossRef]
79. Silva, J.; de Brito, J.; Veiga, R. Recycled Red-Clay Ceramic Construction and Demolition Waste for Mortars Production. *J. Mater. Civ. Eng.* **2010**, *22*, 236–244. [CrossRef]
80. Li, X.; Ling, T.-C. Instant CO_2 curing for dry-mix pressed cement pastes: Consideration of CO_2 concentrations coupled with further water curing. *J. CO2 Util.* **2020**, *38*, 348–354. [CrossRef]
81. Suescum-Morales, D.; Cantador-Fernández, D.; Jiménez, J.R.; Fernández, J.M. Potential CO_2 capture in one-coat limestone mortar modified with Mg_3Al–CO_3 calcined hydrotalcites using ultrafast testing technique. *Chem. Eng. J.* **2021**, *415*, 129077. [CrossRef]
82. Suescum-Morales, D.; Fernández, D.C.; Fernández, J.M.; Jiménez, J.R. The combined effect of CO_2 and calcined hydrotalcite on one-coat limestone mortar properties. *Constr. Build. Mater.* **2020**, *280*, 122532. [CrossRef]
83. Zhao, K.; Liang, Y.; Ji, T.; Lu, Y.; Lin, X. Effect of activator types and concentration of CO_2 on the steel corrosion in the carbonated alkali-activated slag concrete. *Constr. Build. Mater.* **2020**, *262*, 120044. [CrossRef]
84. Vogler, N.; Lindemann, M.; Drabetzki, P.; Kühne, H.-C. Alternative pH-indicators for determination of carbonation depth on cement-based concretes. *Cem. Concr. Compos.* **2020**, *109*, 103565. [CrossRef]
85. Seigneur, N.; Kangni-Foli, E.; Lagneau, V.; Dauzères, A.; Poyet, S.; Le Bescop, P.; L'Hôpital, E.; de Lacaillerie, J.-B.D. Predicting the atmospheric carbonation of cementitious materials using fully coupled two-phase reactive transport modelling. *Cem. Concr. Res.* **2020**, *130*, 105966. [CrossRef]

86. De Hita, P.R.; Pérez-Gálvez, F.; Morales-Conde, M.J.; Pedreño-Rojas, M.A. Characterisation of recycled ceramic mortars for use in prefabricated beam-filling pieces in structural floors. *Mater. Construcción* **2019**, *69*, e189. [CrossRef]
87. Gonçalves, T.; Silva, R.V.; De Brito, J.; Fernández, J.M.; Esquinas, A.R. Mechanical and durability performance of mortars with fine recycled concrete aggregates and reactive magnesium oxide as partial cement replacement. *Cem. Concr. Compos.* **2020**, *105*, 103420. [CrossRef]
88. Lozano-Lunar, A.; Dubchenko, I.; Bashynskyi, S.; Rodero, A.; Fernández, J.; Jiménez, J. Performance of self-compacting mortars with granite sludge as aggregate. *Constr. Build. Mater.* **2020**, *251*, 118998. [CrossRef]
89. Qian, X.; Wang, J.; Fang, Y.; Wang, L. Carbon dioxide as an admixture for better performance of OPC-based concrete. *J. CO2 Util.* **2018**, *25*, 31–38. [CrossRef]
90. Wu, C.-R.; Hong, Z.-Q.; Zhang, J.-L.; Kou, S.-C. Pore size distribution and ITZ performance of mortars prepared with different bio-deposition approaches for the treatment of recycled concrete aggregate. *Cem. Concr. Compos.* **2020**, *111*, 103631. [CrossRef]
91. Dang, J.; Zhao, J.; Pang, S.D.; Zhao, S. Durability and microstructural properties of concrete with recycled brick as fine aggregates. *Constr. Build. Mater.* **2020**, *262*, 120032. [CrossRef]
92. Ye, G.; Liu, X.; De Schutter, G.; Poppe, A.-M.; Taerwe, L. Influence of limestone powder used as filler in SCC on hydration and microstructure of cement pastes. *Cem. Concr. Compos.* **2007**, *29*, 94–102. [CrossRef]